IAEA International Atomic Energy Agency

XRF Newsletter

Newsletter of the IAEA Laboratories, Seibersdorf
Issue No. 25, September 2013

ISSN 1608–4632

X ray Fluorescence in the IAEA and its Member States

In This Issue

Activities in the IAEA XRF Laboratory

Results of the worldwide proficiency test - PTXRFIAEA09 organized by the Nuclear Science and Instrumentation Laboratory

Introduction

One of the main missions of any analytical laboratory is the provision of reliable results. Many X-ray fluorescence laboratories in the International Atomic Energy Agency (IAEA) Member States (MSs) carry out research aimed at improving the performance and extending the applicability of various X-ray based techniques [1].
The IAEA assists its MSs Laboratories to maintain their readiness by producing reference materials, by developing standardized analytical methods and by conducting inter-laboratory comparisons and proficiency tests as tools for quality control. To achieve this aim and ensure a reliable worldwide, rapid and consistent response, the IAEA Nuclear Science and Instrumentation Laboratory (NSIL) organizes proficiency tests annually for X-ray spectrometry laboratories.

Fig. 1. Geographical distribution of the laboratories participating to the PTXRFIAEA09. Thirty-three (33) laboratories from twenty-nine (29) countries submitted their results.

The main objective of these tests is to enhance the capability of interested MSs in effective utilization of nuclear spectrometry and analytical services in industry, human health, agriculture, and in monitoring and evaluation of environmental pollution. Indeed, proficiency tests are designed to identify analytical problems, to support IAEA MSs laboratories to improve the quality of their analytical results, to maintain their accreditation and to provide a regular forum for discussion and technology transfer in this area. The type of samples and the concentration levels of the analytes are designed and chosen in a way to better enable identification of potential analytical problems. Since 2001, the NSIL has organized nine proficiency test exercises (PTXRFIAEA) [2].

2. Methodology and Evaluation of Results

The proficiency test organized in 2012 (PTXRFIAEA09) was aimed at analytical laboratories applying X-ray fluorescence (XRF) techniques in environmental monitoring. River clay samples with established homogeneity and well characterized known target values of the mass fractions of analytes were chosen as test samples and distributed to the participating laboratories. The laboratories taking part in the exercise are graphically shown in Fig. 1.

The mass fraction results received from the participating laboratories were thus analysed in order to provide criteria for the assessment of the quality of the results. Based on the results of the proficiency test presented in the final report, each participating laboratory should assess its analytical performance by using the specified criteria and, if appropriate, to identify discrepancies, and to correct relevant analytical procedures. Each laboratory was assigned a code, therefore full anonymity of the presented results is guaranteed. The link between the laboratory code and the laboratory name is known only to the organizers of the proficiency test and to the laboratory itself.

The reference values supplied by the provider of the material, established by independent inter-laboratory survey, were used as the assigned values of the analytes, X_A. For each analyte a target value of the standard deviation has been assigned using a modified Horowitz function as proposed in the reference [3]:

$$H_A = \begin{cases} 0.22 X_A & X_A < 1.2 \cdot 10^{-7} \\ 0.02 (X_A)^{0.8495} & 1.2 \cdot 10^{-7} \le X_A \le 0.138 \\ 0.01 \sqrt{X_A} & X_A > 0.138 \end{cases} \quad (1)$$

In Eqn. (1) the assigned value of analyte, X_A, is expressed as a mass fraction. The target value of the standard deviation, σ_A is related to H_A by a factor k:

$$\sigma_A = k H_A, \quad k = 0.5, 1.0, 1.5 \quad (2)$$

Depending on the value of the factor k the target value of the standard deviation is recognized as fit-for-purpose at three levels of uncertainty: k = 0.5 - appropriate for high precision analysis; k = 1.0 - appropriate for well-established routine analysis; k = 1.5 - satisfactory for common analytical tasks. The relative value of the target standard deviation, *RSD*, expressed in percent, is defined as follows:

$$RSD = \frac{\sigma_A}{X_A} \cdot 100\% \quad (3)$$

The reported concentrations of analytes were compared with the assigned values by using the z-score analysis. For every result a z-score was calculated:

$$z = \frac{x - X_A}{\sigma_A} \quad (4)$$

The term 'x' denotes the reported mass fraction of analyte. Defined by different fit-for-purpose ranges of the target standard deviation, three different values of z-scores were calculated by combining Eqns. (2) and (4). Assuming that appropriate values for X_A and σ_A have been used and that the underlying distribution of analytical errors is normal, apart from outliers, in a well-behaved analytical system z-scores would be expected to fall outside the range $-2 \le z \le 2$ in about 4.6% of instances, and outside the range $-3 < z < 3$ only in about 0.3%. Therefore, based on the z-scores the following decision limits were established:

$|z| \le 2$: a satisfactory result

$2 < |z| < 3$: the result is considered questionable

$|z| \ge 3$: the result is considered unsatisfactory

The advice to the laboratory is that, independent of the fit-for-purpose range selected by the laboratory, any *z*-score for an element outside the range $-2 \le z \le 2$ should be examined by the analyst and all steps of the analytical procedure verified to identify the source(s) of the analytical bias.

For every participant the rescaled sum of *z*-scores, *RSZ*, as well as the sum of squared *z*-scores, *SSZ*, were calculated as defined by the following equations:

$$RSZ = \frac{\sum_{i=1}^{L} z_i}{\sqrt{L}} \tag{5}$$

$$SSZ = \sum_{i=1}^{L} (z_i)^2 \tag{6}$$

The symbol '*L*' denotes the number of results provided by the laboratory/participant for all the analytes determined. The summing up in Eqns. (6) and (7) takes into account all *z*-scores for all analytes with known assigned values reported by participant. The *RSZ* can be interpreted as a standardized normally distributed variable, with expected value equal to zero and unit variance. It is sensitive in detecting a small consistent bias in an analytical system; however, it is not sensitive in cases where there are even big errors but having opposite signs. The *SSZ* takes no account of the signs because it depends on the squared *z*-scores. It has a chi-squared (χ^2) distribution with *L* degrees of freedom. The *SSZ* can be regarded as complementary to *RSZ*, which means that if *RSZ* is well within the range $-3 < RSZ < 3$ and if at the same time the value of *SSZ* is above the $\chi^2_{critical}$ value, the overall performance of the laboratory requires improvement.

The reported results were accompanied by the standard uncertainty estimate made by the participant. The values were used to calculate *u*-scores:

$$u = \frac{|x - X_A|}{\sqrt{(\sigma_A)^2 + (\sigma_x)^2}} \tag{7}$$

The symbol 'σ_x' denotes the standard uncertainty of the submitted result *x*. If the assumptions about X_A and σ_A and about the normality of the underlying distributions are correct, and the laboratory estimate of σ_x takes into account all the significant sources of uncertainty, the *u*-scores would have a truncated normal distribution with unit variance. In a well-behaved analytical system only 0.1% of *u*-scores would fall outside the range $u < 3.29$. Therefore, the following decision limits for the *u*-scores were established:

$u \le 1.64$: reported result does not differ from the assigned value
$1.64 < u \le 1.95$: reported result probably does not differ from the assigned value
$1.95 < u \le 2.58$: it is not clear whether the reported and assigned values differ
$2.58 < u \le 3.29$: reported result is probably different from the assigned value
$3.29 < u$: reported result differs from the assigned value

The *u*-scores are especially useful for deciding whether the laboratory fit-for-purpose criteria are fulfilled. By comparing Eqn. (4) and Eqn. (7) one can notice that for corresponding values of *u*-score and *z*-score the following inequality is always fulfilled:

$$u \le |z| \tag{8}$$

It implies that if the *u*-score is larger than 3.29 also the decision limit for the corresponding *z*-score is triggered and the laboratory has to check the analytical procedure as well as review the uncertainty budget estimation. If *u*-score stays below the value of 1.64 and at the same time the *z*-score decision limit is triggered ($|z| > 3$) the laboratory should reevaluate its fit-for-purpose status for that particular analyte.

To examine the overall performance of the participating laboratories the submitted results have been statistically processed and the consensus values were calculated. The results were tested for the presence of outliers using a set of seven outlier rejection tests. The results which passed the outlier rejection procedures were used to calculate the consensus mean value of analyte, X_C, and corresponding consensus value of its standard deviation, σ_C:

$$X_C = \frac{\sum_{i=1}^{m} x_i}{m} \tag{9}$$

$$\sigma_C = \sqrt{\frac{\sum_{i=1}^{m}(x_i - X_C)^2}{m(m-1)}} \qquad (10)$$

The term m denotes the number of reported values for a given analyte excluding the outliers rejected by at least one of the outlier rejections tests. The summing up in Eqn. (9) and (10) takes into account only the results which passed all the outlier rejection tests.

3. Results

The River Clay test sample was distributed to 42 laboratories for chemical composition analysis. Out of the 42 laboratories, 33 participated in the test submitting 673 individual results for 58 chemical elements (for 20 of which the assigned values were not available). The consensus values and corresponding standard deviations were calculated based on 587 reported analytical results after excluding 86 results classified as outliers. The correlation between the assigned and the consensus values is shown in Fig. 2.

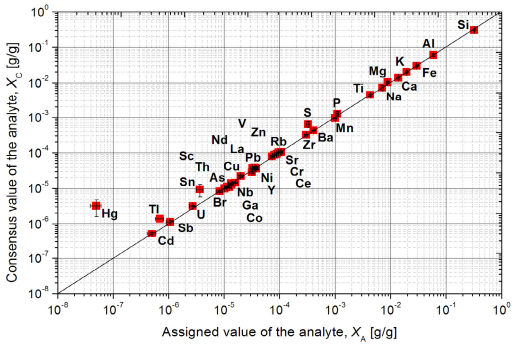

Fig. 2. Correlation between assigned, X_A, and consensus values of analytes, X_C. Solid red squares correspond to the elements the assigned values of which were known with high degree of accuracy. The uncertainties of the assigned values were calculated according to Eqn. (2) with k = 1. The uncertainties of the consensus values were calculated according to Eqn.(20), except for the results reported by single laboratory, in such a case the laboratory estimate of the uncertainty was shown in the plot.

In Fig. 3 the distribution of single element concentrations (for Zr) obtained from different laboratories is shown. For few elements, the result of density distributions shown in Fig. 3 could only be used as indicators of the trends observed in the reported data due to the limited number of results. All the populations of results, after outlier rejection, have passed a normality test (Kolmogorov-Smirnov).

In Fig. 4 the distribution of the results obtained for each element (in this case for Zr) using *z*- and *u*-scores and the discrepancies from the assigned value is shown. The bar chart distributions of the *z*-scores were presented for the analytes with at least 6 submitted results. The results are sorted in ascending order versus laboratory/technique code. The decision levels of satisfactory results, $|z| < 2$, for different fit-for-purpose targets have also been marked.

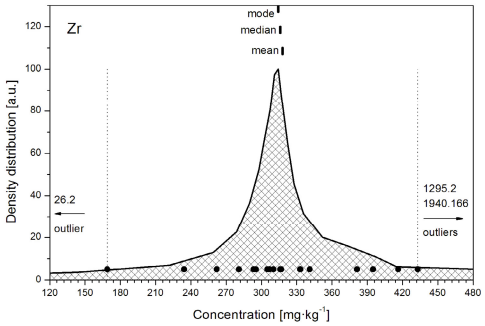

Fig. 3. The density distribution functions for the analyte Zr. The individual results are marked with filled circles. The dotted lines show the range of the accepted results – these results were used to calculate the consensus values. The outliers are marked with arrows. Also shown are the estimated parameters of the distribution (after outlier rejection): mode, median, and the mean value.

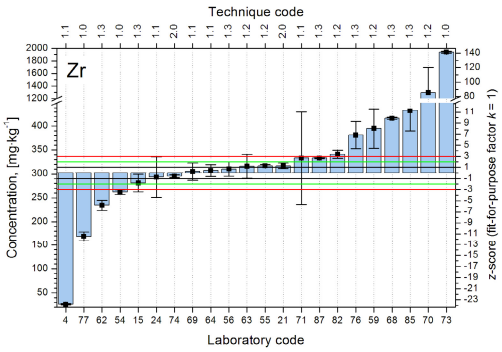

*Fig. 4. Distributions of z-scores for analyte Zr. The bar charts show the distance between the reported and the assigned values of the analyte. The submitted results and their uncertainties, as provided by the analysts, are marked with filled squares accompanied by uncertainty bars. The horizontal lines show the admissible levels of z-score, $|z| < 2$, for three different fit-for-purpose ranges defined by factor k in Eqn. (2): **k = 0.5 - solid black lines**, **k = 1.0 - solid green lines**, and **k = 1.5 - solid red lines**.*

For every participating laboratory its overall performance can also be presented. The plots presented in Fig. 5 relate all the *u*-scores and *z*-scores calculated for a given laboratory. The decision limits of unsatisfactory results were marked with black lines ($|z| > 3$, $u > 3.29$). They divide the plot area in four quadrants. Due to

inequality (8) all the points accompanied by a laboratory estimate of the uncertainty fall always below the line u = |z|. The smaller the laboratory estimate of the uncertainty the closer the related point to the u = |z| line. The well performing laboratories would have more points located in the lower-left quadrant of the plot. If there are many points located in the upper-right quadrant it suggests that these results do not fall in the defined fit-for-purpose targets and that the laboratory provided too "narrow" uncertainty estimate.

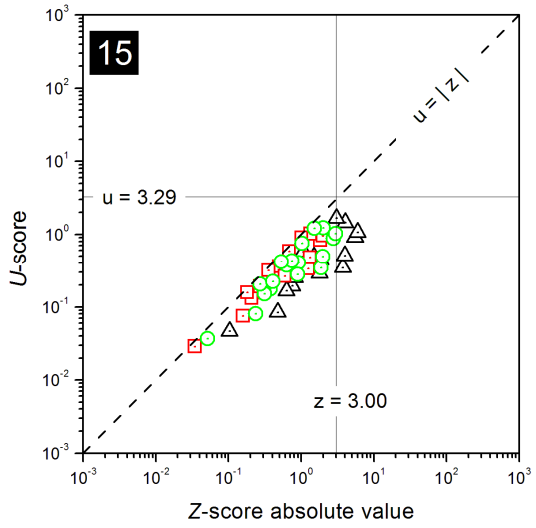

Fig. 5. Combined plots of z- and u-scores for one participating laboratory. The hollow symbols denote the values calculated for specific fit-for-purpose levels as defined in Eqn. (2) with factor k, namely: ***k = 0.5 - black triangles****,* ***k = 1.0 - green circles****, and* ***k = 1.5 - red squares****. The solid lines mark the decision levels for z-score, |z| = 3, and u-score, u = 3.29. Points in the immediate proximity of the dashed diagonal line (u = |z|) have underestimated uncertainty values.*

The partitioning of the results between different analytical techniques is presented in Fig. 6. The largest fraction of analyses, about 83%, was carried out with the energy dispersive spectrometry (EDXRF+TXRF), about 10% with wavelength dispersive mode. Most of the determinations were carried out on samples prepared in the form of pellets (~ 69%), about 5% of the results were obtained after converting the sample to a liquid form by acid digestion or dissolution, about 16% of measurements were carried out on fused beads, and about 10% of analyses were performed without any sample preparation.

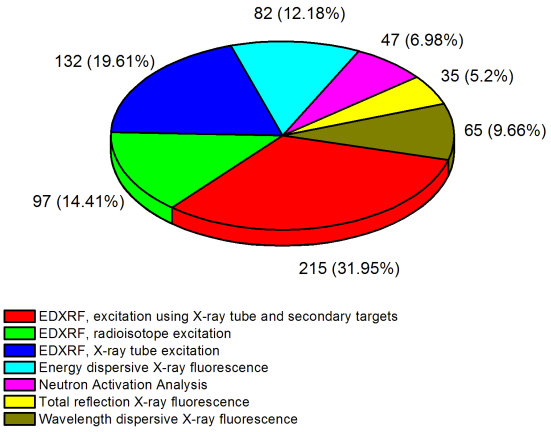

Fig. 6. Utilization of analytical techniques. For each analytical technique the number of submitted results is shown. The per cent values relate to the total number of 673 submitted results.

For more information please contact:
Mr Alessandro Migliori, A.Migliori@iaea.org

References

[1] PADILLA ALVAREZ, R., MARKOWICZ A., WEGRZYNEK D., CHINEA CANO E., BAMFORD S.A., HERNANDEZ TORRES D., Quality management and method Validation in EDXRF analysis, X-Ray Spectrom. 36 (2007) 27-34

[2] http://www.iaea.org/OurWork/ST/NA/NAAL/pci/ins/xrf/pciXRFcurr.php, accessed on 2012-03-26

[3] THOMPSON, M., Recent trends in inter-laboratory precision at ppb and sub-ppb concentrations in relation to fitness for purpose criteria in proficiency testing, Analyst 125 (2000) 385-386

CRP on "Improvement of portable instruments and analytical techniques for in-situ applications", Vienna, April 8-12, 2013

CRP G42004 Coordination Meeting

Considerable progress has been observed in recent years in the design of portable instruments for in-situ applications. The efficiency of the analytical work for studies requiring an extensive sampling has improved considerably by incorporating the in-situ analysis as one of the initial stages in the work. In-situ analysis improves management decisions by providing quasi-real time, densely spaced, and repeatable characterization data. In-situ measurements, although having comparatively less accurate results than laboratory based ones, are a less expensive alternative and allow achieving an effective screening in many studies.
In the cases when taking portions of the samples for laboratory analysis is unfeasible in-situ techniques are the only alternative. When the measurements are conducted in a completely non-destructive way, the techniques become the only alternative for the analysis of valuable or unique objects, such as archaeological findings or valuable art exponents.
Taking into account the importance of the in-situ analytical techniques based on nuclear spectrometry in different fields, the IAEA organized the Coordinated Research Project G42004 on improvement of portable instruments and analytical techniques for in-situ applications in order to coordinate and support the research efforts in this field. The CRP aims at contributing effectively to meet the objectives of the IAEA Regular Budget Project 1.4.3.4, i.e., *to enhance the capability of interested Member States to effectively utilize nuclear spectrometries for analytical services in environmental pollution monitoring and other applications, including nuclear energy system-related needs*. The results of the CRP can be transferred to other laboratories which are not directly participating in/contributing to the CRP leading to a technology and know-how transfer from developed to developing IAEA Member States.
The specific objectives of this CRP are:

- To develop portable instruments featuring more efficient instrumental response, reduction in noise and time signal processing to achieve higher input count rate capabilities and energy resolution, in designs with the lowest possible weight and power demands
- To implement and validate robust analytical procedures including solutions to correct the inaccuracies in the results arising from differences in sample geometry, matrix and other characteristic features of in-situ analysis
- To contribute to enlarge the spectrum of in-situ applications of nuclear spectrometry methods in support of research and technological development in nuclear science and technology, industry, environmental pollution monitoring, among other fields.

The purpose of the meeting was to:

- review the current status of research activities and results obtained by the participating teams in the improvement of portable instruments, analytical techniques and operational procedures for in-situ applications
- update information on the available instruments and facilities that are developed and/or in use in the present CRP
- coordinate the research activities of the present CRP and identify collective needs and actions that could support the implementation of the projects
- Define adjustments required in the program of work for the remaining duration of the CRP.

Representatives of 10 laboratories involved in the CRP (5 Research Contract holders and 5 Research Agreement holders) participated in the meeting, and presented the results achieved so far in the respective projects, including details on the work plan activities foreseen for the future. The following table summarizes the results obtained so far:

Table 1: CRP results

Expected Output	Current Status, April 2013
Improved performance of portable nuclear spectrometers.	ARG16762: A low cost lens to focalize x-rays of conventional (extended focal spot) x-ray tubes was developed BEL16787: The mobile XRF system of the "Centre Européen d'Archéométrie" of the University of Liège has been upgraded and several features of performance optimized: more robust, compact and lighter measuring head, better energy resolution, bigger effective detection area, increased effective solid angle, automatic control of the operational parameters for the detector and the X-ray source, transmission of data via Ethernet cable. An IP camera has been installed to visualize the analyzed zone in real time. The system allows performing 2D elemental mapping in a faster time (2s/spectrum) with good counting statistics. CUB16737: A preliminary design of an excitation module combining long-lived radioisotope sources with secondary targets that could be used in portable XRF spectrometers using Si-PIN or SDD detectors was carried out by means of Monte Carlo (MC) simulations EGY16409: New algorithms were proposed for overcoming pileup and dead time problems in NaI gamma ray spectroscopy and their performance compared to that of other algorithms reported. Development of a neural network based algorithm for detection and correction of pile upped pulses using MATLAB Environment was implemented. ITA16858: The existing spectrometer was upgraded with a new x-ray tube, with a remotely controlled and finely tunable He flushing system and more compact detection geometry is under development to further increase the sensitivity for low Z elements. The home-made list mode acquisition for elemental mapping has been developed and is now under test; the first maps were obtained and the system is under tuning. The design of the lightweight and more compact structure based on carbon fiber is under development. SYR16291: Two configurations of the instrument were designed during the project and tested
New applications in support of research, innovation and technological development.	BEL 16787: The spectrometer has been used in different studies, including the study of Picasso's painting "La Famille Soler". ITA 16858: a new criterion to distinguish between traditionally maintained and artificially renewed ancient Japanese swords (Katana) has been developed ITA16788: preparation of materials suitable to simulate the results of weathering processes and heterogeneity expected for the objects under study. A standard procedure for the analyses of corroded outdoor bronzes was developed and tested. LEB16821: the built-in calibrations of Niton XRF analyser were tested for metallic objects and ceramics. SYR16291: 7 jars and 14 jars from Tell Al- Kroum and Tell Humera

	archaeological sites, respectively, were analyzed
Improved analytical methodologies for in-situ measurements.	ARG16762: a method to characterize the lens transmission and focusing features based on the measurement of the XRF induced in thick multi-elemental targets by polychromatic X-ray excitation was developed CUB16828: The applicability of a Monte Carlo code previously developed for the efficiency calibration of HPGe detectors laboratory in gamma spectrometry measurements (DETEFF) was extended to in situ gamma-ray spectrometry practice, for the determination of ground deposition activity when an uniform distribution of the activity is assumed in different layers JAM16786: MATLAB based contour mapping software was developed for off-line use.

Conclusions

During the meeting the current status in implementation of in-situ analytical techniques was reviewed. The applications of portable instruments cover many fields such as, cultural heritage, environmental pollution monitoring, biomedicine and pharmaceutical control. The ideas presented by the participants provided possible solutions for the particular problems

Potential interactions have been identified among participants with common interests, particularly related to verification of performance of the instruments and external quality control

Publications emerging from the CRP:

Mahmoud I.I. et. al., Pileup Recovery Algorithms for Digital Gamma Ray Spectroscopy, Journal of Instrumentation, Vol. 7, No. 9, 2012.

J. Carrazana González et. al., Application of the Monte Carlo code DETEFF to efficiency calibrations for in situ gamma-ray spectrometry, Appl. Radiat. Isotopes, 70 (2012), pp. 868–871

For more information please contact the IAEA Scientific Officer of the CRP: Mr Padilla-Alvarez, at R.Padilla-Alvarez@iaea.org

Enhancing the Characterization, Preservation and Protection of Cultural Heritage Artefacts, Group Fellowship Training, 4-15 March 2013, Seibersdorf, Austria

IAEA Regional Technical Cooperation Programme RER0034

The aim of the Group Fellowship Training (GFT) course was to provide advanced theoretical knowledge, technical and practical experience for effective utilization of Nuclear Analytical Techniques (NATs) in the characterization of artworks and other Cultural Heritage objects. Methodological aspects were discussed on the utilization of X-Ray Fluorescence analysis, Synchrotron Radiation based and Ion-Beam Analysis techniques in support of Art and Archaeological studies, and special emphasis was given to the benefits and limitations of the portable/handheld XRF instrumentation. Good practices for data analysis and interpretation were presented. The group fellowship training was followed by ten participants from Albania, Bulgaria, Croatia, Greece, Hungary, Romania, Serbia and Ukraine (Fig. 7). Three external experts, Prof. Koen Janssens (University of Antwerpen), Dr. Armando Sole (ESRF, Grenoble) and Dr. Sylvia Calusi (LABEC-INFN, Florence) have contributed in the GFT with lectures and tutorials.

The course was composed of theoretical lectures on the following topics:

- *XRF analysis and modern instrumentation (XRF group/NSIL)*

- *Quantitative XRF analysis using Fundamental Parameters approach (XRF group/NSIL)*
- *Portable XRF analysis of metal objects, ceramics and paintings (XRF group/NSIL)*
- *XANES: principles and case studies in cultural heritage studies (Koen Janssens*)
- *Macroscopic XRF-based imaging of works of art (Koen Janssens)*
- *Absorption and phase contrast tomography and case studies related to glass corrosion and its conservation treatment (Koen Janssens)*
- *XRF/XRD 2D imaging and tomography: XANES vs. XRD imaging with case studies on paint multilayers, vermillion degradation (Koen Janssens)*
- *Introduction to PyMca software for XRF qualitative and quantitative analysis (Armando Sole)*
- *Analytical applications of the PyMca software in the field of Cultural Heritage (Armando Sole)*
- *PIXE/RBS analysis and applications in cultural heritage field (XRF group/NSIL and RBI/Zagreb)*
- *Introduction to the GUPIX software for PIXE quantitative analysis (Silvia Calusi)*
- *Ionoluminescence for materials characterization and application in CH field (Silvia Calusi)*
- *Discussion on alternatives to solve analytical problems faced by the participants at their home institutions (XRF group/NSIL)*

Apart the theoretical presentations, the GFT programme focused on practical demonstrations and hands-on exercises at the IAEA laboratories utilizing the XRF instrumentation of the Nuclear Science and Instrumentation Laboratory (NSIL) and in particular the modular 2D/3D micro-XRF spectrometer and a handheld XRF analyser. Representative archaeological samples such as glazed ceramics, metallic alloys, and pigments were examined and methodological aspects were discussed regarding the optimization of the XRF measurements, data analysis and interpretation. In parallel, two tutorials were conducted offering hands on practice on the utilization of PyMca software for XRF quantitative analysis and imaging (by Dr. Armando Sole, see Fig. 8) and on GUPIX for PIXE quantitative analysis (by Dr. Silvia Calusi).

The GFT programme participants visited the scientific laboratory of the Kunsthistorisches Museum in Vienna (KHM) for a whole day. During the morning session Dr. Martina Grießer informed the GFT participants of the KHM activities in the field of non-destructive analyses of artwork and cultural heritage artifacts, while Dr. Katharina Uhlir gave an overview of the use of the micro-XRF spectrometer PART-II. During the afternoon session the participants had the great opportunity to visit the Antiques Collection and Ephesus Museum of the KHM and conduct in-situ measurements using the NSIL handheld XRF analyzer (Fig. 9). These analyses were conducted on the selected artefacts for the first time and aimed to identify on the remaining polychromy the pigments palette used for the surface decoration of the ancient marble sculptures.

Finally, the GFT programme included a demonstration of Ion Beam Analysis techniques through a remote live connection with the accelerator facility at the Rudjer Boscovic Institute (RBI) in Zagreb. Dr. Milko Jaksic, Dr. Stjepko Fazinic and Mr Natko Shukan ran the accelerator and conducted characteristic PIXE/RBS experiments. The acquired spectra were presented in real time in Seibersdorf, while the RBI colleagues explained the various spectral features emphasizing the pros and cons of IBA techniques versus XRF methods. The contributions provided by the external experts and the RBI and KHM teams were extremely valuable for the successful completion of the GFT programme and are highly acknowledged.

For more information you can contact Mr Andreas Germanos Karydas who has been acted as Course Director (A.Karydas@iaea.org). The NSIL team that has contributed to the GFT programme included Dr. Roman Padilla-Alvarez and Dr. Alessandro Migliori.

Acknowledgements: The support of the IAEA TC team responsible for the organization of the workshop is highly acknowledged and in particular of Ms Rodriguez Y Baena Alesssia Maria, Mr Padilla Alvarez Roman, Ms Cueto Ruby and Mr Lukumbuzya Kaseza.

Fig. 7. The NSIL instructors and GFT participants of the RER0034 Training Course at the IAEA Laboratories at Seibersdorf. In the middle, the Section Head of the Physics Section Prof. Ralf Kaiser (IAEA) is shown together with the invited expert Dr. Sylvia Calusi (INFN, LABEC)

Fig. 8. The GFT participants during a tutorial hands-on tutorial on the quantitative XRF analysis and imaging software PyMca given by the invited expert Dr. Armando Sole (ESRF).

Fig. 9. In-situ XRF analysis of ancient marbles polychromy utilizing a handheld XRF analyzer (performed by Dr. Velibor Andric, Serbia) at the Antiques Collection and Ephesus Museum of the Kunsthistorisches Museum in Vienna (KHM)

Joint ICTP-IAEA Workshop on Advanced Synchrotron Radiation based X- ray Spectrometry Techniques, 22 to 26 April 2013, ICTP, Trieste, Italy

The Abdus Salam International Centre for Theoretical Physics (ICTP) in cooperation with the IAEA organized a Workshop in Trieste entitled "*Advanced Synchrotron Radiation based X- ray Spectrometry Techniques*", from 22 to 26 April 2013. The Directors of the workshop were Andreas Germanos Karydas (IAEA), Burkhard Beckhoff (Physikalisch-Technische Bundesanstalt, Berlin) and Diane Eichert (Elettra Sincrotrone Trieste) with Joe Niemela as local organizer (ICTP).

The workshop was organized in support of the IAEA and the ICTP efforts to strengthen the capacity of scientists from developing countries to effectively utilize advanced X-ray Spectrometry (XRS) techniques at Synchrotron Radiation facilities by fostering their education and training and facilitating their access to a synchrotron beamtime. The workshop overviewed the current advances in Synchrotron Radiation (SR) based X-Ray Spectrometry (XRS) techniques, discussed future developments and offered a forum to exchange crosscutting information among the participants. Particular emphasis was given to analytical XRS applications in materials science, nanoelectronics, environmental sciences and biomedicine. The following topics were addressed in the workshop program:

- X-ray Optics (Alex Von Bohlen/*ISAS, Dortmund*), Status and trends in photon detection (Ralf Menk/*Elettra, Trieste*)
- Reference free X-ray Spectrometry (Burkhard Beckhoff/*PTB, Berlin*)
- Introduction to X-ray Absorption Spectroscopy (XAS): XAFS and XANES, theory (Sakura Pascarelli/*ESRF, Grenoble*)
- Fundamentals and Analytical Applications of Grazing Incidence and Total Reflection XRF Analysis (GIXRF-TXRF) for nanoscaled materials characterization (Giancarlo Pepponi/*FBK, Trento* and Matthias Muller/*PTB, Berlin*), Environmental (Janos Osan and Szabina Torok/*KFKI, Budapest*) and Biomedical applications (Christina Streli/TUW, Vienna)
- Buried nano-layer and interface analysis by GIXRF-NEXAFS (Beatrix Pollakowski/*PTB, Berlin)*
- High energy resolution x-ray photon-in photon-out spectroscopy (Matjaz Kavcic/*JSI, Ljubljana*)
- Correlating Synchrotron Radiation Techniques as a tool for life science research (Diane Eichert/*Elettra, Trieste*)
- Confocal X-ray microscopy: Principle and analytical applications (Andreas Germanos Karydas/*IAEA, Vienna*)

The workshop programme included several tutorials on particular topics related to the scope of the workshop, whereas some of them were conducted in the computer room of ICTP supporting hands on practice and exercises:

- Quantitative XRF (Michael Mantler/*Rigaku Corporation, Tokyo*)
- Quantitative GIXRF (Beatrix Pollakowski/*PTB, Berlin*)
- XAS data analysis (Giuliana Aquilanti/*Elettra, Trieste*) and
- PyMca software for XRF analysis (Armando Solé/*ESRF, Grenoble*)

Thirty four participants attended the workshop from many different regions (Latin America, Europe, Africa, Middle East and Asia-Pacific). (see Fig. 10)

Fig. 10. The participants of the ICTP-IAEA workshop during the visit at Elletra Sincrotrone Trieste

The opportunities opened for the IAEA member states to access the X-Ray Fluorescence (XRF) beamline and the IAEA UHVC end-station of the Elettra Laboratory, Sincrotrone Trieste, were presented and disseminated during a Round table discussion chaired by Burkhard Beckhoff (PTB) with the objective to stimulate the creation of a 'user community.' The panel contributors were B. Beckhoff (PTB), A. Karydas (IAEA), D. Eichert (ELETTRA), M. Kiskinova (ELETTRA), J. Niemela (ICTP) and H. Hoorani (SESAME). A questionnaire was prepared and distributed to the participants to express interest regarding the need for basic or advanced training, applications

areas, analytical aspects and specific synchrotron radiation techniques. In particular, the round table discussion included the following topics:

1. advanced training needs of workshop participants (based on the survey results)
2. research interests of workshop participants (based on the survey results)
3. support schemes for access to SR by workshop organizers
4. open discussion on training schemes and research implementation

As a follow up activity, a school is scheduled to be organized again at ICTP in cooperation with the IAEA and Elettra Sincrotrone Trieste from 17 November to 28 November 2014. The school is entitled: "*Joint ICTP-IAEA School on Novel Experimental Methodologies for Synchrotron Radiation Applications in Nanoscience and Environmental Monitoring*" and aims mainly to provide hands-on training and experience in the utilization of various synchrotron radiation techniques.

For more information the IAEA Scientific Officer of the CRP you can contact Mr Andreas Germanos Karydas (A.Karydas@iaea.org)

Fig.11. Participants of the ICTP-IAEA workshop during a tutorial on XAFS software given by Dr .Giuliana Aquilanti (Elettra Sincrotrone Trieste)

Final Coordination meeting of the CRP G42003 (2010-2013) entitled: "Micro-analytical techniques based on Nuclear Spectrometry for Environmental monitoring and Material Studies"

Laboratori Nazionali del Sud Istituto Nazionale di Fisica Nucleare, Catania, Italy, 27-31 May 2013

In 2009 the IAEA initiated a coordinated research project (CRP) on '*Micro-analytical Techniques Based on Nuclear Spectrometry for Environmental Monitoring and Material Studies*" under the project 1.4.3.4. Nuclear Spectrometry for Analytical Applications. The major objective was to assist laboratories in Member States with enhancing/improving the proper and effective utilization of nuclear spectrometries and analytical services in industry, human health, agriculture and environmental pollution monitoring through new and extensive (broad range) applications of micro-analytical techniques. It was expected that the results of the proposed CRP could be used both by small laboratories in the developing Member States and state-of-the-art synchrotron radiation facilities available in the developed countries and also that could be transferred to other laboratories which will not participate in/contribute to the CRP directly.

The specific research objectives of the CRP included:

1. improved instruments for analytical methodologies and standardized procedures utilized by micro-analytical techniques based on nuclear spectrometry,
2. applications of micro-analytical techniques for 2D and 3D microscopic imaging and element-specific analysis complemented by chemical speciation in support of research and technological development in nuclear science and technology, industry, environmental pollution monitoring, production of reference materials etc.

The CRP covered a period of almost four years (2010–2013). Sixteen laboratories from both developed and developing Member States participated including the IAEA's Laboratories. The first research coordination meeting (RCM) was held at the International Atomic Energy Agency (IAEA) premises in Vienna, from 17 to 21 May 2010. The participants presented progress reports on research activities in the field of microanalytical techniques based on nuclear spectrometry, reviewed the status of the instrumentation and methodologies available, agreed on a detailed work plan for the CRP and identified potential synergies among the participating groups, with common interests, particularly related to cultural heritage and environmental studies.

The second RCM was held again in Vienna from 17 to 21 October 2011. The participants reviewed and summarized the research results of the CRP achieved so far, and reported new outcomes in areas related to characterization of air pollution, elemental pollution of soils and water, cultural heritage and preventive conservation, material analysis, microanalysis of biological and biomedical materials, actinide elements in nuclear materials and confocal X ray systems. Finally, the participants created new collaborations across nuclear spectrometry based micro-

analytical techniques and their applications that will benefit both the participants and other Member States.

The third RCM was organized in Laboratori Nazionali del Sud Istituto Nazionale di Fisica Nucleare, Italy from 27 to 31 May 2013. The participants reviewed and summarized the specific CRP research outputs (see Table 2), assessed the impact of the CRP and identified and recommended outstanding research areas that may be worthwhile to follow up after the CRP. Finally, the participants provided various recommendations to the IAEA and Member States on how the field of microanalytical techniques based on nuclear spectrometry can follow up technological developments and meet the needs of MS to address analytical problems in various intersdisciplinary fields. The IAEA Scientific Officer of this CRP was Mr Andrzej Markowicz (2010-2012) and for 2013 Mr Andreas Germanos Karydas.

Table 2: Summary of the CRP outputs

Country	Improvements in the analytical performance of micro-analytical techniques	Standardized analytical procedures including optimized sample preparation techniques	Modern (upgraded) instruments and analytical methodologies including software packages for data acquisition and data evaluation	New applications in support of research, innovation and technological development
Australia	A modified 3-DRUM PM2.5 strip sampler has been developed, two 3DRUM sampling units have been operational for 36 months, monitoring dust storm events across east and northwest coasts of Australia. We have written an improved PIXE code to simulate X-ray yields from micro-PIXE in coincidence with a focused X-ray confocal detection systems.		Upgraded laser absorption techniques for black carbon strip filter measurements with millimeter resolution, developed automated laser absorption techniques for black carbon measurements on DRUM strips providing 6 hrs timing resolution. Developed new confocal X-ray focused PIXE system with 10 micron resolution.	Combined HYSPLIT wind speed and direction data with IBA elemental data for the first time to identify dust sources from agricultural regions. Current work is looking at dust movements across the NW coast and effects of dust on the Great Barrier Reef and coral systems. Combined positive matrix factorization methods with wind back trajectory data to determine both source types and source locations.
Argentina		Analytical procedures for soil analysis. Optimization of sample preparation for soils, hair and blood analysis. Improved QA/QC procedures. Soil analysis and cultural heritage in collaboration with other countries.		Procedure for toxic element determination in biological tissues. Improving portable XRF spectrometer for cultural heritage and environmental applications.
Austria	Improved GI-XRF software: combined GIXRF and XRR fitting	development of GI-XRF and XRR measurement protocols	GI-XRF tested for As implants and HfO2 thin layers	SR-TXRF XANES of Fe and Rh in human cells; Sr uptake in trabecular bone of Sr-treated rats; Pb, Zn, Sr, Ca distribution in human osteoporotic bone samples
Belgium		Sampling and analytical procedures for atmospheric aerosols and gaseous pollutants		Preventive conservation studies finalized in 15 museums and cathedrals (of which 4 in cooperation with Argentina and Portugal) and preliminary study of atmospheric particle interactions with pigments. Multi-techniques studies with Argentina of ancient human bones, leather, ceramics and pigments
Croatia	New PIXE/RBS end-station with improved analytical capabilities; Measurements of uncertainty budget for PIXE analysis of particulate matter (PM) samples in collaboration with the IAEA Laboratories Seibersdorf	Calibration for particulate matter analysis by using new PIXE/RBS chamber	New gas ionization detector for heavy ion RBS re-installed at a dedicated chamber. Simple gas ionization detector for STIM constructed and tested; Axial gas ionization detector for ERDA designed; Miniature HR PIXE spectrometer for use at the ion microprobe designed, constructed and tested.	Ray-tracing study of downsized HR PIXE spectrometer design for chemical speciation performed; HR-PIXE operational at the ion microprobe
Greece	Sample preparation and investigation procedures for alloys of biomedical interest developed and adopted. Corrosion measurements of surface modified Ti-6Al-4V and	IBA and corrosion procedures for alloys of biomedical interest tested and adopted	Continuation of the Tandem VdG facilities improvement – proton microprobe installed but not yet operational	Testing of corrosion resistance of surface modified alloys of biomedical interest

	sion measurements on real CoCrMo orthopedic implants initiated. Particle microprobe installed but not yet operational for measurements			
Greece	Batching mode of XRF/PIXE spectra de-convolution and quantitative procedure for 2d mappings	Calibration protocols-procedures based on the Fundamental Parameter Approach for PIXE, Sy-XRF and tube-excited XRF set-ups	An integrated GUI software for quantitative analysis of PIXE and XRF modes has been developed	
Italy	Portable XRD measurements for large d-spacing minerals completed. Full Filed XRF with high energy and high spatial resolution developed. Low-Energy micro-XRF installed and commissioned	Improvement of the combined use of the portable alpha-PIXE and portable XRD for the pigments analysis confirmed by applications	Developed new high intensity 210-Po source for PIXE, constructed and tested new modular portable-XRD system, developed an X-ray pinhole camera.	Compositional and mineralogical investigation of ancient pigments from different cultures and historical periods.
Poland	Software for chemical composition evaluation of individual particles with micro-XRF based on Monte Carlo simulation, Monte Carlo simulation-based software for determination of element concentration profiles in layered samples with confocal XRF microscopy, a simple approach for the determination of element concentration profiles of stratified materials by confocal X-ray fluorescence spectrometry, with the use of the direct deconvolution of the measured depth-dependent X-ray fluorescence intensity signals and the established response function of the spectrometer.	Quantitative analysis of thin layers of botanical and biomedical samples with the use of XRF micro-spectroscopy, calibration procedures for analysis of thin samples, development of new reference materials for μXRF spectroscopy	Developed confocal 3D micro-XRF spectrometer and software for data processing, developed measurement control and data acquisition software for the 2D/3D micro-XRF spectrometer Improved laboratory infrastructure based on confocal XRF microscope	Investigation of matrix effect in XRF analysis of individual particles, investigation of the homogeneity of titanium layers in support to biomedical research, quantitative determination of the concentration profiles of Fe and Cu in multilayer polymer samples – validation of the Monte Carlo simulation software, investigation of the biosorption of toxic metals by aquatic accumulators and evaluation of bioremediation efficiency by of applying submerged plants, elemental chemical micro-imaging of human tissues affected by neoplastic processes for investigation of biochemical reactions involved in cancerogenesis.
Portugal		Analytical procedures for paper standard reference samples, samples analysed by EDXRF tri-axial spectrometer, PIXE and TXRF analyses performed, analysis by portable spectrometer done		Upgrade the portable X-ray micro-EDXRF system, new detector with thin Be window for detection low-Z elements installed
Slovenia	Developed preliminary quantification software for low energy micro-XRF analysis		Quantification of low energy micro-XRF scanning for light elements was developed, tested and validated	Application of X-ray based techniques in the research of plant ionomics for food biofortification, phytoremediation and toxicity of nano-materials
South Africa	achieved capability of micro-PIXE analyses of biological thin and semi-thick sections in frozen-hydrated state	Sample preparation and measurement procedures adapted for specific applications indicated in the plan of work		Biofortification of staple food crops completed; plant-yeast symbiosis completed, study on fruit disorders completed, Ni speciation in hyper-accumulators completed within the scope defined for CRP
Sri Lanka		Developed procedures for microwave digestion for rice analysis by TXRF technique	Analysis of soil samples by EDXRF, analysis of rice samples by TXRF, collection of rice samples	
Ukraine	Improvement of the high-brightness electron source providing submicron spot sizes, improvements of the high-brightness ion source		Development of the anode cooling system in proton-beam induced X-ray source, development of X-ray optics with polycapillary lens	Calculation and measurement of proton-induced X-ray yield
United Arab Emirates	Installing of 50 μm capillary x-ray guide in the μXRF system instead of 10 μm capillary for increased intensity, efforts are being made to setup a micro RAMAN system.		Raman, XRD, FTIR and SEM systems installed and applied to environmental and cultural heritage, new aerosol sampling capabilities are acquired	Study of ”dust particle” effect on museum showcases performed; study of size-resolved elemental distributions of aerosol particles, sourcing of air pollutants continues, regional collaboration for

				aerosol pollution mapping started.
USA	Demonstrated integration of conventional 2D MXRF with 2D hiRX technique and 3D confocal MXRF with high sensitivity and selectivity for elemental characterization	Developed novel small volume (pL) deposition for instrument calibration and sample characterization	Developed hiRX prototype instrument utilizing MWDXRF technology with novel doubly curved crystals (DCC)	hiRX application for actinide element characterization specifically uranium and plutonium

Conclusions

This CRP has applied nuclear methods and related techniques to produce new outcomes not reported previously in areas related to characterization of air pollution, elemental pollution of soils and water, cultural heritage and preventive conservation, material analysis, microanalysis of biological and biomedical materials, actinide elements in nuclear materials and confocal X-ray systems.

Some of these new outcomes include:

- New information on relative contributions of agriculture and farming to extreme desert dust storm events experienced annually along the east coast of Australia
- Applied new high resolution X-ray (hiRX) methodology for direct actinide element characterization of nuclear materials
- Development of a new high efficiency portable alpha-PIXE spectrometer and new modular portable-XRD system and their application for the non-destructive characterization of ancient mineral pigments
- Construction of 2D/3D confocal XRF microscope and the measurement control/data acquisition software for the characterization of biological and multi-layered multi-element samples
- Size, elemental concentration and source apportionment of aerosol particulate matter in the United Arab Emirates was determined for the first time
- By combining complementary analytical methods available in different countries more complete characterization of critical pollutants in residential areas was achieved in Argentina
- Ion Beam Analysis techniques in combination with electrochemical corrosion testing lead to the assessment of the corrosion resistance of surface-modified metallic alloys for biomedical applications and contributed to the improvement of their properties
- New software has been developed for batch analysis of XRF/PIXE spectra de-convolution and quantitative procedure for 2D mappings
- Application of X-ray based techniques in the research of plant ionomics for food biofortification, phytoremediation and toxicity of nano-materials
- Development of improved high-brightness electron source providing submicron spot sizes, improvements of the high-brightness ion source.

The participants (see Fig. 12.) have created new and enduring collaborations across nuclear spectrometry based micro-analytical techniques and their applications that will benefit both participants and MS.

A total of 122 refereed journal publications, 18 conference proceedings, 131 conference contributions, 10 book chapters and 13 reports have been produced by the CRP participants to date to publicize their research outcomes nationally and internationally. This significant number of journal articles and conference presentations allowed dissemination of the information beyond the borders of the CRP for the benefit of the wider research community.

For more information please contact the IAEA Scientific Officer of the CRP Mr Andreas Germanos Karydas (A.Karydas@iaea.org)

Fig. 12. The participants of the RCM in Catania

X ray Fluorescence in Member States

India

Micro-beam X-ray fluorescence spectroscopy using Indus-2 synchrotron radiation facility: beamline BL-16

Contributors: M. K. Tiwari,* G. S. Lodha and S. K. Deb
Indus Synchrotrons Utilization Division, Raja Ramanna Centre for Advanced Technology, Indore-452013 (M P), India
*Email: mktiwari@rrcat.gov.in

Indus-1 and Indus-2, are India's national synchrotron radiation facilities located at Raja Ramanna Centre for Advanced Technology (RRCAT), Indore. Indus-1 is a 450 MeV electron storage ring which provides synchrotron radiation in the VUV soft x-ray range with a critical wavelength of 61 Å whereas Indus-2 is a 2.5 GeV, 300 mA synchrotron radiation machine with a critical wavelength of 2 Å for its bending magnet source. The Indus-2 is at present operating at 2.5 GeV, 100 mA in round-the-clock operation mode. Both synchrotron sources exist in the same premises of RRCAT, Indore and have very good air/rail connectivities with major cities of India. The RRCAT centre also fosters research and development activities in the fields of particle accelerators, Lasers and related advanced technologies like cryogenics, ultra high vacuum, superconducting cavities, RF power, magnet and their application in different fields of science, thus the centre provides a unique platform covering a wide range of experiments for the synchrotron users in the Indian subcontinent.

Considering the several advantages of the synchrotron based microfocus x-ray fluorescence (μ-XRF) technique [1-4] and to fulfil the requirements of the XRF spectroscopy users of universities and various research laboratories in India, a μ-XRF beamline (BL-16) has been built at the Indus-2 synchrotron radiation source with an experimental emphasis on atomic physics, fundamental parameters (FP) evaluation for quantitative x-ray fluorescence analysis, environmental, archaeological, biomedical and material science applications involving heavy metal speciation and their localization. The beamline is installed on a bending-magnet source and works in the x-ray energy range 4–20 keV. It provides both microfocused and collimated beams at the experimental station. BL-16 beamline offers a wide range of measurement capabilities which include; microprobe XRF examination of a specimen for spatial distribution of elements, energy dispersive x-ray fluorescence (EDXRF) analysis and total reflection x-ray fluorescence (TXRF) characterization of materials at ppb (parts per billion) levels with a short spectrum acquisition time. In addition to the elemental mapping, BL-16 beamline also allows a user to perform other modes of XRF characterization, viz; grazing incidence x-ray fluorescence (GIXRF) analysis, chemical speciation, near-edge absorption spectroscopy and x-ray reflectivity measurements of thin layered materials etc. The details of the BL-16 beamline are given elsewhere [5].

The BL-16 beamline began user operation in mid-2011. Since then it has been used for a variety of research applications by the Indian universities users pertaining to studies on the effect of fertilization process on the chemical environment of elements in plants [6], micro XRF studies of (U, Th) O2 pellets [7], determination of tantalum impurity contents in superconducting Niobium metal [8], validation of XRF inversion code for Chandrayaan-1 mission [9], determination of x-ray intensity ratios and Resonant Raman Scattering (RRS) cross sections across the absorption edges of elements, etc.

Fig. 1. A front view of the Indus complex, at RRCAT, Indore, India

Fig. 1 presents the front view of the Indus complex which comprise of Indus-1 and Indus-2 synchrotron sources. Fig. 2a depicts the photograph of the microfocus x-ray fluorescence beamline (BL-16) of Indus-2. The inset of Fig. 2a illustrates the schematic optical layout of the beamline. The radiation shielding hutch of the beamline and the built in personal safety interlock system allow the safe operation of the beamline. The beamline operates under high vacuum condition (vacuum ~ 1×10-6 mbar).

The optics of the BL-16 beamline comprises of a double crystal monochromator (DCM) with Si(111) symmetric and asymmetric crystals (mounted side-by-side), a Kirkpatrick-Baez (KB) focusing optics and the combination of slits in order to reduce the scattered x-ray background reaching to the experimental station which usually concocts from different optical elements of the beamline. The experimental stations of BL-16 beamline consist of a 5-axes sample manipulator for microprobe XRF–scanning applications, XRF and TXRF setups and a 2-circle goniometer for x-ray reflectivity and GIXRF characterization of thin layered materials. All the experimental stations of the BL-16 beamline have been setup in such a manner so that they can be operated independently without disturbing each other. The BL-16 beamline provides photon flux of the order of ~ 106-107 ph/sec/100mA in the microfocused beam mode.

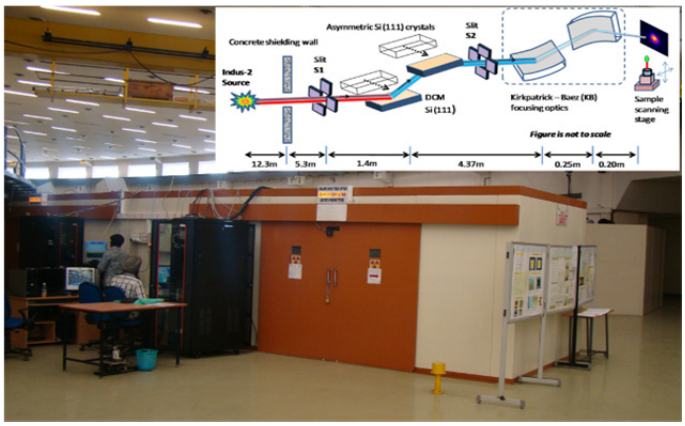

Fig. 2a. Photograph of the microfocus x-ray fluorescence beamline (BL-16) of Indus-2 synchrotron radiation facility. In the inset of figure a schematic optical layout of the beamline is shown.

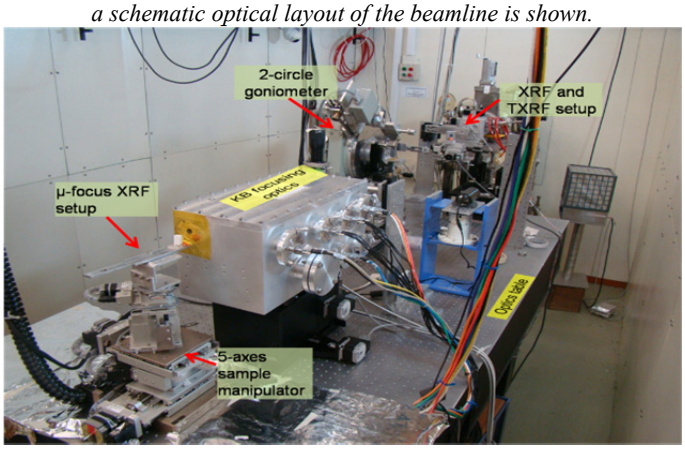

Fig. 2b. Inside view of the experimental hutch of the BL-16 beamline, showing various experimental stations installed on the beamline.

Fig. 2b demonstrates inside of the experimental hutch of the BL-16 beamline, showing various experimental stations of the beamline. Several detectors (ionization chamber, avalanche photodiode, single element energy dispersive SDD detector, MiniFdi and VHR x-ray CCD cameras) are also available on the BL-16 beamline that make possible to record good quality x-ray fluorescence data. Fig. 3 illustrates a CCD image of the microfocused beam generated at the 5-axes sample manipulator stage of the BL-16 beamline. The measured vertical and horizontal dimesnions of the microfocused beam was found to be ~ 4.3μm (V) × 7.5μm (H).

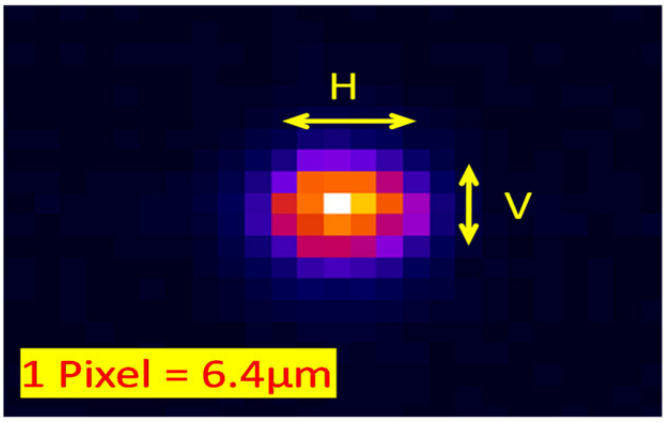

Fig. 3. A CCD image of the microfocused beam generated from the KB system of the BL-16 beamline at the 5-axes sample manipulator stage.

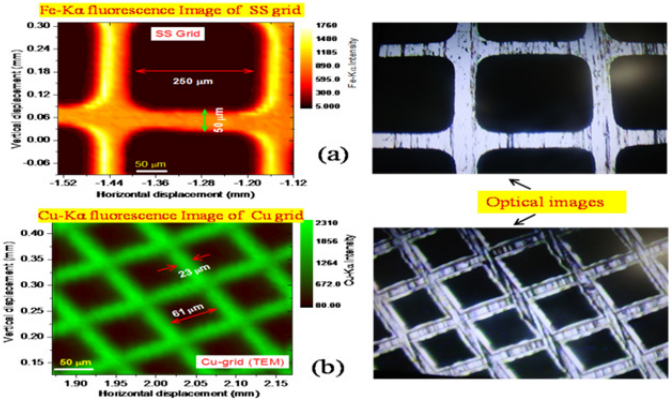

Fig. 4. Measured fluorescence micrographs of different test grid structures using the BL-16 microfocus beam. (a) Stainless steel grid structure (b) a Cu grid structure. On the right hand side of the figures corresponding optical image of the grid structures are shown.

To bench mark μ-fluorescence mapping capabilities of the BL-16 beamline a few test pattern structures (grid structures) have been examined. These grid structures were mounted on the 5-axes sample manipulator stage, close to the focal spot of the KB optics. Fig. 4 shows the two-dimensional elemental fluorescence maps of the Stainless Steel (SS) grid and a Cu grid structures. These maps were generated by measuring net area intensities of Fe-Kα and Cu-Kα fluorescence lines respectively. The measured fluorescence images of the grid structures were also compared with their optical images. The observed dimensions of the grid structures obtained from the μ-fluorescence measurements were found to match closely with the optical measurements.

One of the potential features of the BL-16 beamline is that it allows various re-configurable operational modes (normal XRF, TXRF and μ-XRF modes) with a minimal setup time which enables a wide range of experiments to be performed on the beamline.

Around the activities of BL-16 beamline, we have also developed and setup laboratory based XRF instrumentations, (viz. EDXRF and TXRF spectrometers) to support offline XRF analysis and to perform pre-characterization of the user's samples before going to an actual synchrotron beamtime application.

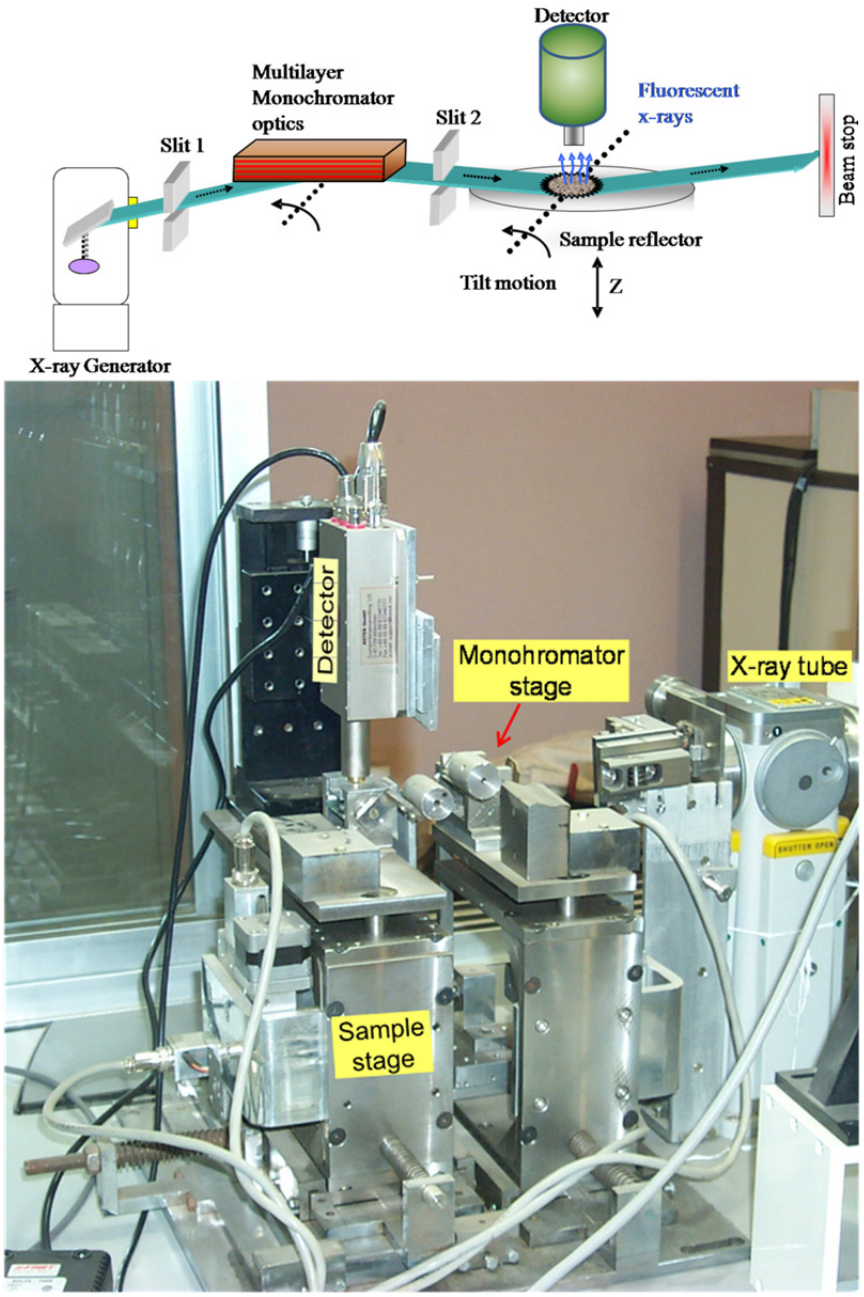

Fig. 5. Photograph of the TXRF spectrometer developed at RRCAT, Indore. On the top of figure a schematic optical layout of the spectrometer is shown.

Fig. 5 shows the photograph of the TXRF spectrometer, which has been developed in our laboratory [10]. To set very small grazing incidence angles required in TXRF, indigenously built precise linear and rotation stages have been used rather than using commercially available expensive motorized-goniometers. The mochromator stage and the sample carrier stages have been provided provisions for independent angular and vertical translation motions. The angular tilt motions on the two reflector stages have been provided by means of sin-bar mechanism that gives almost backlash free angular adjustment with a 0.001 degree angular resolution. The provision of independent vertical translation and precise angular motions of the two reflector stages facilitates the use of any x-ray tube energy as well as variety of primary beam modification units like cut-off reflector, multilayer monochromator or natural crystal monochromator in the TXRF spectrometer. This indigenously developed simple and precise TXRF spectrometer has been used for variety of research applications [11-15]. Laboratory based TXRF system provides element detection sensitivities in the range of 2-200 ppb on the other hand synchrotron TXRF measurements offer sub-ppb detection sensitivities for most the elements.

Extensive efforts have also been made for the development of quantitative analysis procedures for EDXRF and grazing incidence x-ray fluorescence (GIXRF) techniques for characterization of bulk samples and thin periodic multilayer structures. We have developed a computer program called 'CATGIXRF' [16] for the calculation of GIXRF intensities originated from thin layered materials (single and multilayer films coated on polished substrates). This program has been used for variety of applications including impurity depth profiling inside Si wafers and float glass substrates and for the x-ray standing wave (XSW) characterization of diverse types of multilayer structures for their interface diffusion and roughness effects [17-20]. The 'CATGIXRF' program has also been freely distributed to researchers of various countries on their requests.

We anticipate that with the help of existing beamline infrastructure and the laboratory based XRF instrumentation, it is possible to cater to the needs of a wide synchrotron XRF user community in the region of the Indian subcontinent.

References:

[1] IIDA, A., NOMA, T., Synchrotron X-ray muprobe and its application to human hair analysis, Nucl. Instrum. Methods Phys. Res. B 82 (1993) 129–138.

[2] NEWVILLE, M., SUTTON, S.R., RIVERS, M.L., ENG, P., Micro-beam X-ray absorption and fluorescence spectroscopies at GSECARS: APS beamline 13ID, J. Synchrotron Rad. 6 (1999) 353–355.

[3] YOUNG, L.W., WESTCOTT, N.D., ATTENKOFER, K. and REANEY, M.J.T., A high-throughput determination of metal concentrations in whole intact Arabidopsis thaliana seeds using synchrotron-based X-ray fluorescence spectroscopy, J. Synchrotron Rad. 13 (2006) 304-313.

[4] HARRIS, H.H., VOGT, S., EASTGATE, H., LEGNINI, D.G., HORNBERGER, B., CAI, Z., LAI, B. LAI, P.A., Migration of mercury from dental amalgam through human teeth, J. Synchrotron Rad. 15 (2008) 123-128.

[5] TIWARI, M.K., GUPTA, P., SINHA, A.K., KANE, S.R., SINGH, A.K., GARG, S.R., GARG, C.K., LODHA, G.S., DEB, S.K., A microfocus X-ray fluorescence beamline at Indus-2 synchrotron radiation facility, J. Synchrotron Rad. 20 (2013) 386–389.

[6] KAUR, K., DEEP, K., BANSAL, M., TIWARI, M.K., MITTAL, R., Peak energy shift with fertilization in mint plants: EDXRF measurements with synchrotron photon source, Archives of Applied Science Research, 4 (5) (2012) 2152-2160.

[7] MISRA, N.L., TIWARI, M.K., SANJAY KUMAR, S., DHARA, S., KUMAR SINGH, A., LODHA, G.S., DEB, S.K., GUPTA, P.D., AGGARWAL, S.K., Synchrotron-induced EDXRF determination of uranium and thorium inmixed uranium–thorium oxide pellets, X-Ray Spectrom., 42 (2013) 4–7.

[8] ROY, S.B., SHARATH CHANDRA, L.S., CHATTOPADHYAY, M.K., TIWARI, M.K., LODHA, G.S., MYNENI, G.R., A study on the effect of tantalum-impurity content on the superconducting properties of niobium materials used for making superconducting radio frequency cavities, Supercond. Sci. Technol. 25, (2012) 115020.

[9] ATHIRAY, P.S., SUDHAKAR, M., TIWARI, M.K., NARENDRANATH, S., LODHA, G.S., DEB, S.K., SREEKUMAR, P., DASH, S.K., Experimental validation of XRF inversion code for Chandrayaan-1, Submitted to the journal of Planetary and Space Science (2013).

[10] TIWARI, M.K., SAWHNEY, K.J.S., GOWRI SANKAR, B., RAGHUVANSHI, V.K., NANDEDKAR, R.V., A Simple and precise TXRF spectrometer: construction and its applications, Spectrochimica Acta Part B 59 (2004) 1141– 1147.

[11] TIWARI, M.K., NAYAK, M., LODHA, G.S., NANDEDKAR, R.V., Determination of X-ray compression efficiency of a thin film X-ray waveguide structure using marker layer fluorescence, Spectrochimica Acta Part B 62 (2007) 137-144.

[12] MODI, M.H., LODHA, G.S., TIWARI, M.K., RAI, S.K., MUKHARJEE, C., MAGUDAPATHY, P., NAIR, K.G.M., NANDEDKAR, R. V., Ion irradiation damage on tin side surface of float glass, Nucl. Instr. Method B. 239 (2005) 383-390.

[13] TIWARI, M.K., MODI, M.H., LODHA, G.S., SINHA, A.K., SAWHNEY, K.J.S., NANDEDKAR, R.V., Non-destructive surface characterization of float glass: X-ray reflectivity and grazing incidence X- ray fluorescence analysis, Journal of Non-Crystalline Solids 351 (2005) 2341–2347.

[14] TIWARI, M.K., NAIK, S.R., LODHA, G.S., NANDEDKAR, R.V, Effect of Energy Dependence of Primary Beam Divergence on the X-ray Standing Wave Characterization of Layered Materials, Analytical Sciences, 21 (2005) 757-762.

[15] TIWARI, M.K., SINGH, A.K., SAWHNEY, K.J.S., Sample preparation for evaluation of detection limits (DLs) in X-ray fluorescence spectrometry, Analytical Sciences, 21 (2005) 143-147.

[16] TIWARI, M.K., LODHA, G.S., SAWHNEY, K.J.S., Applications of the 'CATGIXRF' computer program to the grazing incidence X-ray fluorescence and X-ray reflectivity characterization of thin films and surfaces, X-Ray Spectrom. 39 (2010) 127–134.

[17] TIWARI, M.K., BHALERAO, G.M., BABU, M., SINHA, A.K., MUKHERJEE, C., Investigation of metal nanoparticles on a Si surface using an x-ray standing wave field, J. Appl. Phys.103 (2008) 054311.

[18] TIWARI, M.K., SAWHNEY, K.J.S., LEE, T., ALCOCK, S.G., LODHA, G.S. Probing the average size of the self-assembled metal nanoparticles using x-ray standing waves, Phys. Rev. B 80 (2009) 035434.

[19] TIWARI, M.K., SAWHNEY, K.J.S., LODHA, G.S., Characterization of trace embedded impurities in thin multilayer structures using synchrotron X-ray standing waves, Surf. Interface Anal. 42 (2010) 110–116.

[20] TIWARI, M.K., WANG, H., SAWHNEY, K.J.S., NAYAK, M., LODHA, G.S., X-ray standing wave induced Compton and elastic scattering from thin periodic multilayer structures, Phys. Rev. B 87, (2013) 235401.

Italy

Analysis of metal artefacts from the Moche tomb of the "señora de Cao" in the north coast of Peru

Contributors: Roberto Cesareo [(1)], Angel Bustamante D. [(2)], Julio Fabián S. [(2)], Sandra Zambrano A. [(2)], Régulo Franco Jordán [(3)], Arabel Fernandez L. [(3)]

Universita´ di Sassari, Italy and Istituto per lo studio die materiali nano strutturati, CNR-Montelibretti, Rome, Italy

Universidad Nacional Mayor de S Marcos, Lima, Peru

PACEB Museo Cao (Fundación Wiese), Trujillo, Peru

In the north coast of present-day Peru (Fig. 1) between the Andes and the Pacific Ocean, several relevant cultures prospered approximately between 1000 BC and 1375 AD,; among them: Chavín (1000-200 BC), Vicús and Frías (200 BC - 300 AD), Moche (400 BC-700 AD), Sicán (700-1375 AD). These cultures are interconnected and characterized by a high metallurgical ability, demonstrated by the presence of beautiful artefacts such as gold, silver and copper alloys, ceramics and frescos. In this sense the most important culture was surely that of the Moche (or Mochica) , which flourished in the Moche and Chicama valleys, where its great ceremonial centers have been discovered and produced painted pottery, monuments and gold ornaments. The Moche was known as sophisticated metal-smiths, both in terms of their technology, and the beauty of their jewels. The Moche metalworking ability was impressively demonstrated in 1987 when Walter Alva and co-workers discovered the "Tumbas Reales de Sipán" [1] and in 2006 when Regulo Franco discovered the tomb of the "Lady of Cao"[2] (Fig. 2). Spectacular gold and silver funerary ornaments were excavated, and are now displayed in the Museum "Tumbas Reales de Sipan" in Lambayeque, and in the site Museum of Cao, close to Trujillo. The Lady of Cao is a mummy and it is believed she governed the north of present Peru in the 4th century AD. Its discovery, which can be compared with that of the Lord of Sipán, was made by a team of Peruvian archaeologists led by Régulo Franco Jordán of the National Cultural Institute of Peru with the financial cooperation of Foundation Augusto N. Wiese. Before this discovery, it was thought that only men had held high positions in ancient Peru. It is believed that the lady had the status of ruling theocratic in the society Chicama river valley, besides being considered almost divine. The luxury of the decorations and costumes that accompany the funerary bundle of women confirmed the high status of the ruler.

The story of El Brujo and Lady of Cao as told by archaeologists is of one magic and intrigue. The historical pyramid and the female mummy have continued to intrigue historians even today. Located close to the sea, the El Brujo pyramid still stands, and still amazes visitors due to its legends. Although there were other religious and administrative centers in and around the valley, like the Temple of the Sun and the Moon near Trujillo, this particular complex stood out.The other minor centers were constructed to resemble the El Brujo complex. However one of the most stunning relics of civilization is without doubt the site presumably built for the Lady of Cao.

More than 100 metal artefacts were analyzed from the tomb of the Lady of Cao, 60 of them gold or partially gold, 47 silver or partially silver, 23 gilded copper, 5 of tumbaga (poor gold alloys subject to depletion gilding) and 1 of arsenical copper.

A portable EDXRF-system was employed, composed of a mini X-ray tube with a Ag-anode, working at 40 kV and 200 μA maximum voltage and current[3], and a 123-Si-drift detector (Fig. 3**)**, with a 500 μm thick, 20 mm^2 Si-crystal, and a thin Be-window, of 12.5 μm. The energy resolution is 125 eV at 6.4 keV (www.Amptek.com). The X-ray tube irradiates and analyzes an area of about 5 mm diameter when the object is at a distance of 2-3 cm; it is then filtered with barium and collimated. For calibration, Au-Ag-Cu alloys were employed; gold leaves (each Au-foil 0.125 μm thick) and silver foils, (each Ag-foil 0.28 μm thick) were used to simulate the "silvered copper" or "Ag-tumbaga". Calibrated Au-leafs were used, along with several gilded-copper samples with calibrated gilding thickness. Thick sheets of pure gold, copper and silver were also employed.

Fig. 1. Map of the sites of the Moche civilization (with permission of "Fundación Wiese")

Fig. 2. Pyramid "Huaca Cao Viejo" with a view of the tomb of the Lady of Cao (with permission of Fundación Wiese)

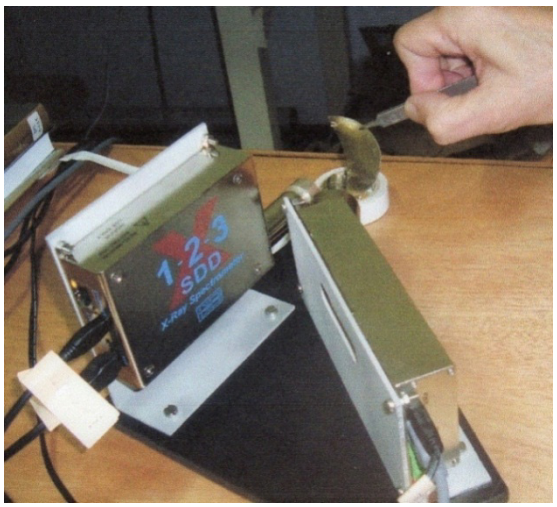

Fig. 3. EDXRF-portable equipment composed of a Si-drift detector (left) and a Ag-anode X-ray tube. Electronics, including bias supply and MCA are in the case of the 123 SDD module

To differentiate gold, gilded copper and tumbaga, the ratios Cu(Kα/Kβ), Au(Lα/Lβ) and Au-Kα/Cu-Kα were employed[3,4]. These ratios may vary for a given element:

- when the element is not in an "infinitely thin" form (self-attenuation effect);
- when a layer of a different material is covering the element (attenuation effect)

The theoretical background of these processes was presented and discussed in many papers[3]. Figures 4-6 show, for example, the self-attenuation curve for Au, the behaviour of Cu(Kα/Kβ)-ratio versus Au-thickness and the curve of Au-Kα/Cu-Kα ratio for gilded copper respectively.

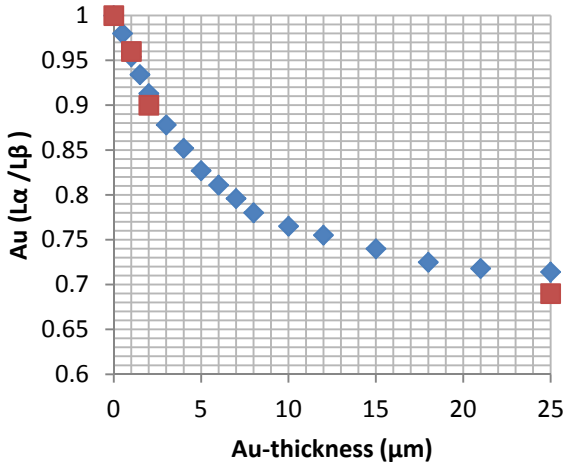

Fig. 4. Au(Lα/Lβ)-ratio versus Au-thickness, normalized to 1 for an infinitely thin sample, according to equation 1 ; theoretical and experimental values are shown as rhombs and squares respectively

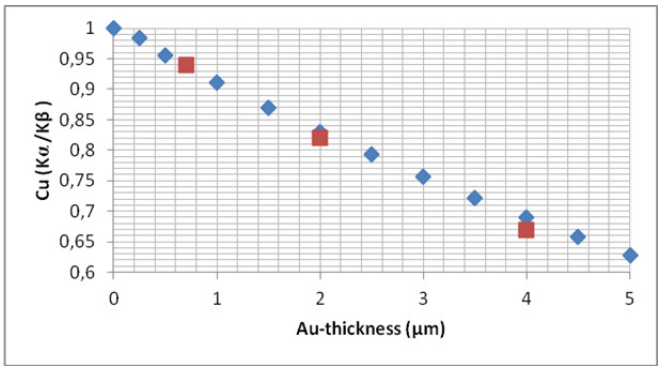

Fig. 5. Cu (Kα/Kβ)-ratio versus Au-thickness, normalized to 1 (no Au), according to equation 2; theoretical and experimental values are shown in blue and red respectively

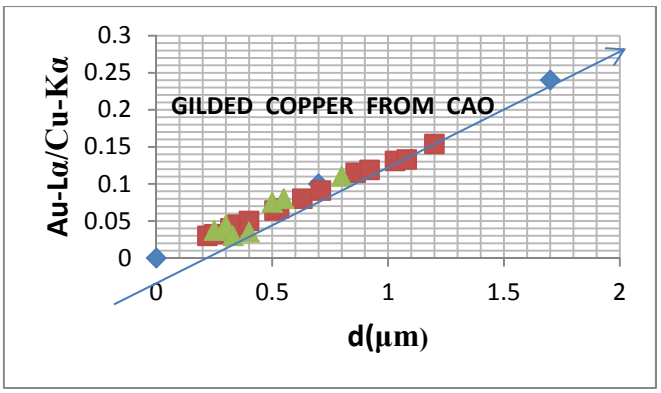

Fig. 6. Au-Lα/Cu-Kα)-ratio versus Au-thickness in the case of gilded-Cu; values for standard samples are shown in blue; experimental values are shown in red and green.

The results of the measurements are presented:

Gold-alloys

The 33 artefacts composed of Au-alloy + Ag-alloy (n.1-33, Figures 7 and 8) and the 11 of Au-alloy, have the same composition, within experimental errors and variations due to ageing processes. The mean values are:
Au = (77.8 ± 4)%
Ag = (17.5±3.5)%
Cu = (4.7±1.3)%

Silver-alloys

The Ag-areas of the same 33 artefacts (Figures 7 and 8) have the following mean composition:
Ag=(70 ± 14)%
Cu=(14 ± 8)%
Au=(16 ± 8)%
The composition of these Ag-alloys is inconsistent, which could be due to different oxidation and enrichment processes during the Centuries. The relatively high content of Au is peculiar, but could be due to the resistance to oxidation.
The 6 small heads (Figure 9) are different, the Ag-composition is constant:
Ag = (98.8±0.5)%
Cu = (1.0±0.5)
Au = (0.2±0.2)%

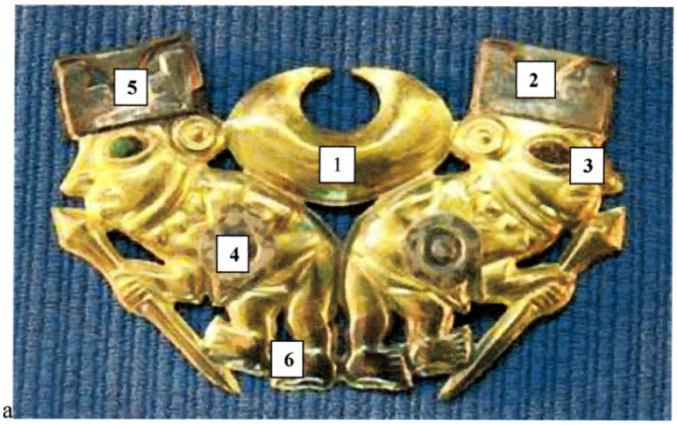

Fig. 7. Object N. 1 composed partially on a gold-alloy (areas 1, 3, 4 6) and partially on a silver-alloy laminar layers (areas 2 and 5).

Fig. 8. Object N. 32 composed partially on a gold-alloy (area 1) and partially on a silver-alloy laminar layers (area 2).

Fig. 9. Object N. 38 on almost pure silver. The analyzed area is indicated. The surface blackening due to oxidation is clearly visible.

Gilded-copper

For the many gilded copper objects (Fig. 10), the following gilding thickness was determined (Fig. 4-6):
d(Au-gilding) = (0.55 ± 0.25) µm with values between 0.25 and 1.2 µm
and mean gilding composition:
Au = (87.5±4)%
Ag = (12.5±4)%.

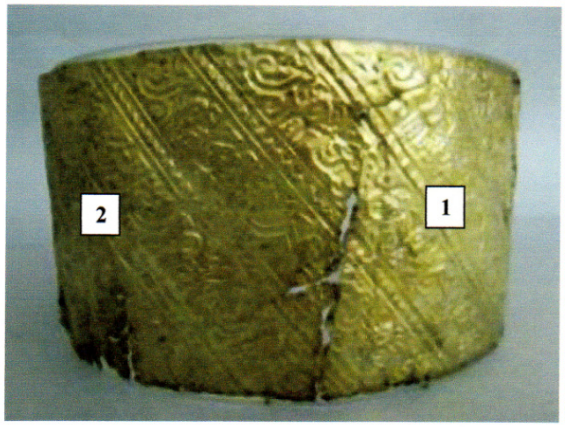

Fig. 10. Object N. 67 on gilded copper. The analyzed areas are indicated.

Tumbaga-objects

Tumbaga was the name given by the Hispanics to a poor gold alloy treated with depletion gilding, producing a thin layer of nearly pure gold by removing the other metals from its surface. The external aspect of a tumbaga-object is quite similar to gold. However, the gold-concentration rapidly decreases with depth after 5-10 µm. Five objects were analyzed and identified as tumbaga (Fig. 11), and in this case copper was removed from the surface; the results are as followed:
d(Au-gilding equivalent) = (3.5 ± 1.0) µm
and mean gilding composition:
Au = (82±3)%
Ag = (18±3)%

Fig. 11. Object N. 87, possibly on tumbaga. All 12 heads were analyzed.

On the basis of Cu(Kα/Kβ), Au(Lα/Lβ) and Au-Kα/Cu-Kα , gold, gilded copper and tumbaga could be clearly differentiated (Fig. 12).

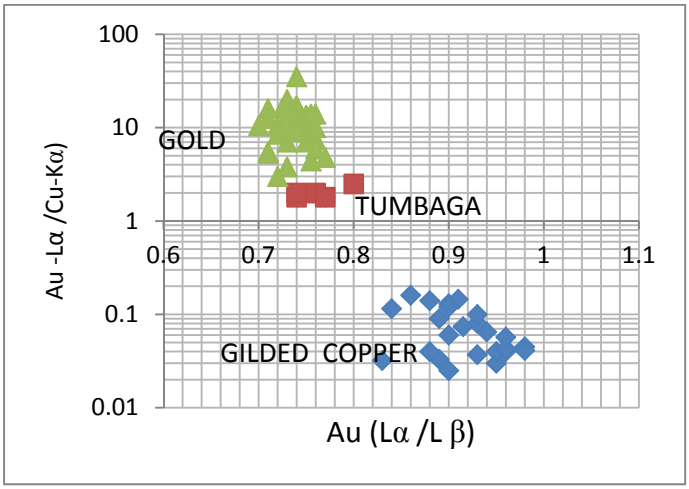

Fig. 12. Gold, gilded copper and tumbaga, differentiated on the basis of Au(Lα /Lβ) and Au-Lα/Cu-Kα ratios;Also the ratio Cu(Kα /Kβ) was usefully employed for differentiation.

References

1. ALVA, W., SIPAN discovery and research, Quebecor Peru 2003, S.A. Lima, Peru
2. MAKOWSKI, K., PILLSBURY, J., JORDÁN, R.G.F, La Señora de Cao. En "Señores de los reinos de la luna". Edición de Krzysztof Makowski, Lima, Banco de Credito del Peru, pp. 280-287.
3.CESAREO, R., BUSTAMANTE, A., FABIAN, J., CALZA, C., DOS ANJOS, M., LOPES, R.T., ALVA, W., CHERO, L., ESPINOZA CORDOBA, M.C., VASQUEZ, R.G., RUIZ, R.R, FERNANDEZ, M.S., Portable equipment for a non-destructive analysis of pre-Columbian metal artefacts from the Royal Tombs of Sipan by energy dispersive X-ray fluorescence spectrometry ; X-Ray Spectrometry 40 (2011) 37-46.
4. CESAREO R., BUSTAMENTE A., FABIAN J., ALVA W., CHERO L., ESPINOZA M., RODRIGUEZ R., SECLEN, M., GUTIERREZ, F., LEVANO, E.B., GONZALES, J., RIZZUTTO, M.A., POLI, E., CALZA C., DOS ANJOS, M., LOPES, R.T., GIGANTE, G.E., INGO, G.M., RICCUCCI, C., ELERA C., SHIMADA, I., CURAY, V., CASTILLO, M., LOPES, F., Evolution of pre-Columbian metallurgy from the north of Peru studied with a portable non- invasive equipment using energy-dispersive X-ray Fluorescence analysis;J. Materials Science and Engineering, B1, July 2011, 48-81.

Italy

FULL FIELD X-RAY FLUORESCENCE IMAGING WITH HIGH-ENERGY AND HIGH-SPATIAL RESOLUTION

Contributors: F.P. Romano [1], L. Cosentino[2], S. Gammino[2], D. Mascali[2], N. Masini[1], L. Pappalardo[1], F. Rizzo[2]
IBAM, CNR, Via Biblioteca 4, 95124 Catania, Italy
INFN-LNS, Via S. Sofia 62, 95123 Catania, Italy
*Email: romanop@lns.infn.it

Abstract

A full field X-ray camera for the X-Ray Fluorescence imaging of materials with high-energy and high-spatial resolution was designed and developed. The system was realized by coupling a pinhole collimator with a position-sensitive CCD detector. X-Ray fluorescence is induced on the samples by irradiation with an external X-ray tube. The characteristic X-ray spectra of the investigated materials are obtained by using a multi-frames acquisition in single-photon counting. The energy resolution measured at the Fe-Kα line was 157 eV. The spatial resolution of the system was determined by the analysis of a sharp-edge at different magnification values; it was estimated to be 90 μm at a magnification value of 3.2x and 190 μm at 0.8x. The present set-up of the system is suited to analyze samples with dimensions up to 5x4 cm^2. Typical measurement time is in the range between 1h to 4 h.

Introduction

The interest in non-destructive elemental mapping of materials by the use of the micro-XRF technique has grown rapidly in a number of scientific disciplines [1-3]. Generally, the X-ray fluorescence micro-analysis is performed by scanning the sample surface through a series of local measurements. The advantages in using this experimental approach were largely demonstrated, even if one limit can be found in the long measurement time necessary for the measurements.
Recently, the development of full field X-ray Fluorescence spectrometers suited for the two-dimensional XRF imaging, represented a novel and promising technique in material studies [4-6].
This work presents a new full field X-ray camera developed at the LANDIS laboratory of the INFN-LNS and IBAM-CNR in Catania (Italy) [7]. A CCD camera, divided into 1024 x 1024 pixels (each pixel presenting a 13 x 13 μm^2 active area and a 40 μm thickness), is used as position- and energy-sensitive detector for X-rays in the range between 3 keV and 30 keV. A 70 μm pinhole-collimator is placed between the sample and the CCD to perform the XRF imaging. Samples are irradiated by a medium power X-ray tube. The X-ray fluorescence, induced on the samples by the primary radiation, is detected with the CCD detector by using a multi-frames acquisition in single-photon counting. An automated post-processing of the data allows to obtain the X-ray fluorescence spectra and, consequently, to perform the two-dimensional elemental mapping of the investigated materials. The energy resolution of the full field X-ray camera is 157 eV at the Fe-Kα line. A spatial resolution was measured at different magnifications. A value of about 90 μm was obtained at a magnification of 3.2x.

Experimental Set-up

The full field X-ray camera installed at the LANDIS laboratory is shown in Fig. 1. It consists of an external X-ray source, the pinhole-collimator and the CCD detector. The CCD, the pinhole-collimator and the sample are arranged in a coaxial geometry in a 50 cm long linear-guide. The samples can be moved along the linear-guide by using manual movements; also, the pinhole-CCD distance can be varied between 10 mm and 80 mm. This set-up allows the easy framing of the samples and the proper selection of the magnification to be used during the measurements.
The primary X-ray source for irradiating the samples is a W anode X-ray tube with maximum working parameters of 50 kV and 2 mA. Irradiation geometry of the samples (i.e. angles and distances) is not fixed but it is determined by the sample position along the linear guide. A 70 μm pinhole-collimator is axially placed between the sample and the CCD detector. The pinhole presents a 75 μm thickness and it is included between two lead foils of 50 μm thickness and presenting a 500 μm central hole.
A back-illuminated and deep depleted CCD camera is used as position- and energy-sensitive detector; it consists of a 13.3x13.3 mm^2 chip divided into 1024x1024 pixels, each one presenting a lateral size of 13x13 μm^2 and a thickness of 40 μm. A removable 25 μm Be window, acting as light-tighter, is installed in the front of the CCD; this absorber strongly reduces the detection efficiency of the CCD in the low energy domain (i.e. below 3 keV).

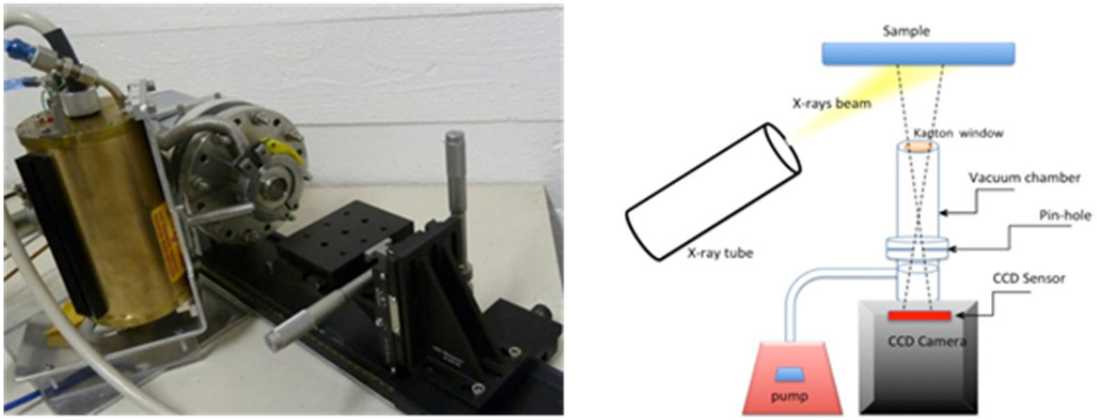

Fig 1. The new X-ray pinhole camera installed at the LANDIS laboratory.

A small volume in front of the CCD sensor is maintained under vacuum during the measurements. This cools the detector down to a temperature of -100 °C with a strong reduction in dark noise.
All the acquisition parameters of the CCD are software-controlled. Exposure time can be fixed down to a minimum value of 10 μsec. The readout process of the CCD is a based on clocking values that can be fixed at 50 kHz and at 1, 3 and 5 MHz. Finally, the 1024x1024 pixels can be binned down to 128x128 pixels. This way measurement time is strongly reduced, even if the spatial resolution results slightly degraded.

Energy Dispersive X-Ray Fluorescence measurements

The spectroscopic capabilities of the full field X-ray camera were investigated by measuring pure target-materials. Since a linear relation is expected between the charge induced on the CCD by the characteristic X-rays emitted by the targets and the energy, these measurements served to calibrate the system and to determine the energy resolution.
The XRF measurements were performed by using a multi-frames acquisition in single-photon counting. The single-photon counting condition is obtained by setting the exposure-time of the single-frame, short enough to have a low number of quanta impinging on the detector. This way each frame will present only a small number of illuminated pixels (about 10-15%) with respect to the total (more than 10^6 in our CCD). Consequently, the probability of a double-hit in the same pixel during the exposure-time of a single-frame can be considered negligible. Sometimes, a single-photon-event interests more than one pixel; these events are recognizable in the frame by the presence of small groups of illuminated neighbor pixels. They are corrected during the post-processing of the data.
Figure 2a shows the energy calibration of the CCD detector performed by the use of the pure targets. Figure 2b presents the spectrum of a pure Fe sample; the energy resolution at Fe-Kα line is 157 eV.

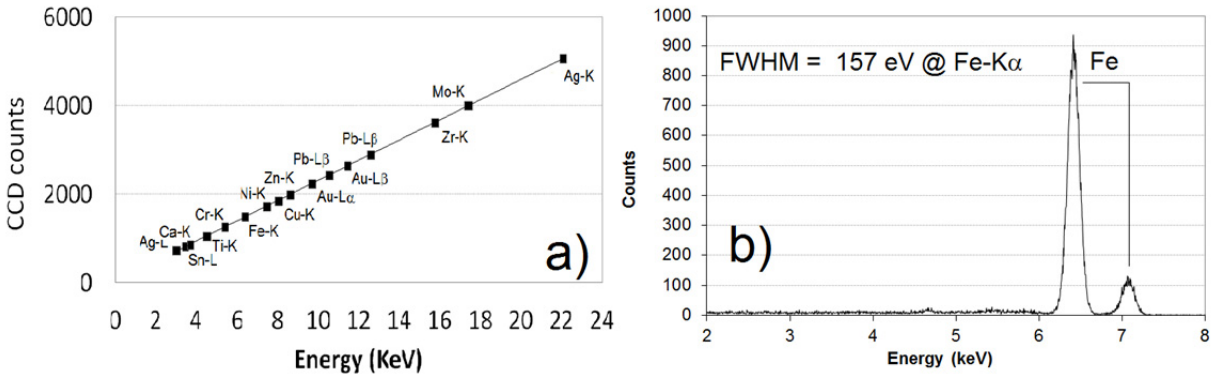

Fig. 2. Energy response of the CCD detector (a) and the energy resolution at Fe-Kα line (b).

Spatial resolution measurements

The spatial resolution of the full field X-ray camera was determined by the analysis of the profile function obtained from a sharp-edge reference-sample. A detailed description of the applied procedure is reported in references [7].

The sharp-edge was realized by covering a 5x5 cm^2 copper plate with a laser-cut tungsten layer of 20 μm thickness; the region of the sample corresponding to the separation edge between copper and tungsten, was irradiated at 35 kV and 1 mA. Measurements on the sharp-edge were performed at the magnification of 3.2x and 0.8x. According to the procedure of references [8, 9],

the profile function of the sharp-edge was fitted with a sigmoidal function. This approach allowed to calculate the Line Spread Function (LSF) and, consequently, to estimate the spatial resolution. Fig. 3 shows the LSF at the magnification of 3.2x and 0.8x.

Spatial resolution evaluated by measuring the FWHM of the LSF was 92 μm at a magnification of 3.2 x and 190 μm at a magnification of 0.8x (Figure3).

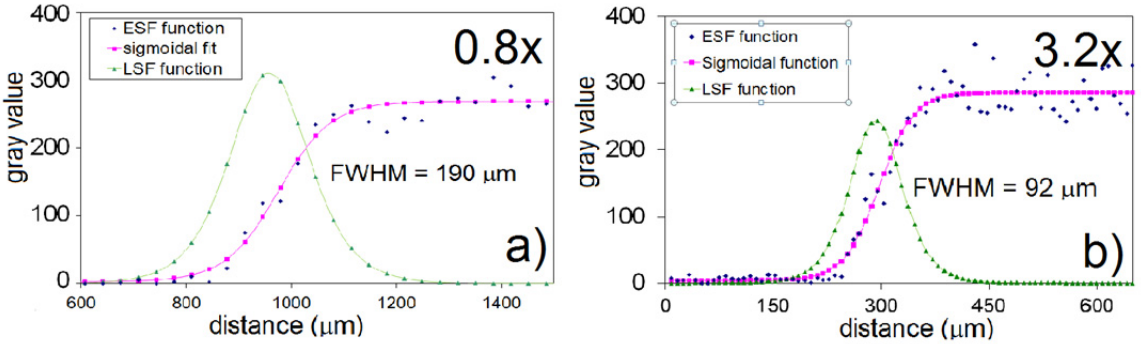

Fig. 3. The LSF functions at 0.8x and 3.2x magnifications. Spatial resolution, i.e. the FWHM of the LSF, is 190 μm at 0.8x and 92 μm at 3.2x.

Full Field X-Ray Fluorescence Imaging

The X-ray spectra measured by using the full field X-ray camera contain information on the lateral distribution of the chemical elements composing the sample under investigation. This aspect was demonstrated by performing the XRF imaging of reference-patterns of different materials and dimensions. Results are reported on ref. 7.

In this paper we present a preliminary result of the application of the full field X-ray imaging technique in the analysis of cultural heritage materials and, in particular, in pigment analysis.

A fragment of painted pottery coming from the Nasca site of Chauachi (Peru) was analyzed by using the full field X-ray camera. This typology of polychrome pottery was realized by the Nasca culture by using the technique of the fired slips. The pigments were manufactured by mixing the coloring substances with clays and, then, fired at high temperature.

The investigated sample is shown in Figure 4a. The 2.5x3 cm^2 area of the painted sample was irradiated by using a broad X-ray beam emitted by the tube equipping the system; a scintillator screen allowed to verify that the sample was homogeneously illuminated by the primary radiation.

In order to frame the entire sample on the 13.3x13.3 mm^2 CCD detector, the magnification was fixed at 0.25x by fixing the sample-pinhole and pinhole-CCD distances at 60 mm and 15 mm respectively. The multi-frame procedure described in the previous sections was applied in a measurement lasted about 2 h.

Figure 4b shows the X-ray spectrum of the investigated sample; K, Ca, Ti, Mn and Fe are clearly visible. Since the low detection efficiency of the CCD at low energy, the Si and Al composing clays are not detected. The characteristic X-ray spectra contain spatial information on the emitting elements. Consequently, the use of appropriate ROI limits in the fluorescence peaks in the spectra, allows investigation of the distribution of the corresponding elements on the irradiated area of the sample.

Fig. 5 shows the result of the Ca, Mn and Fe distribution on the pottery fragment. It is evident that the white pigment is mainly composed of Ca while the black one is composed of a mixture of Fe and Mn.

It is important to note that the irradiation of the sample is not limited to its surface and, consequently, the analytical results contain information both on the painted layer and on the substratum.

Nevertheless the full field XRF imaging can be considered a powerful approach to have fast information on elements characterizing pigments with high lateral resolution. This way the long scansions of the surface performed by using the standard micro-XRF analysis can be avoided.

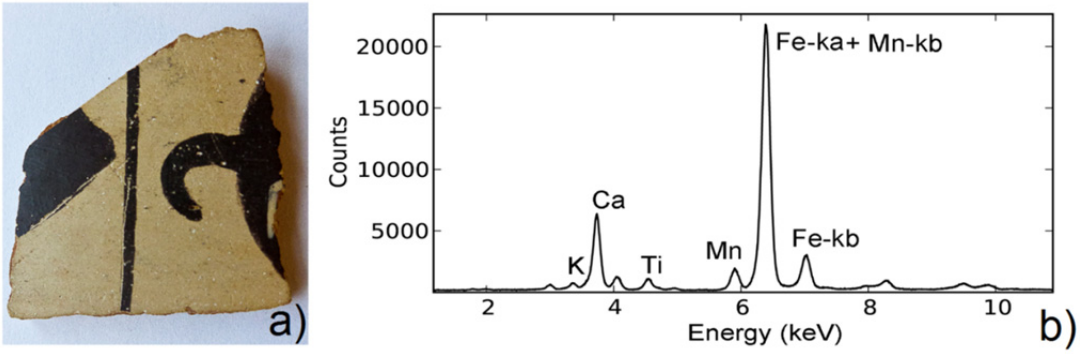

Fig. 4. The investigated Nasca sample (a); and the fluorescence spectrum obtained during the measurement (b).

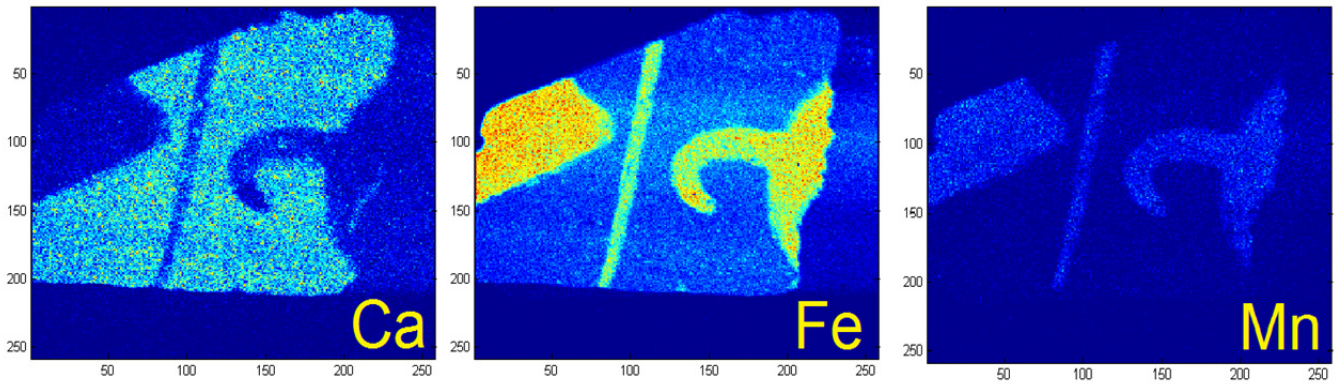

Fig. 5. The elemental distribution of the irradiated pottery; the white pigment is mainly characterized by calcium the black one by iron and manganese.

Conclusions

A new full field X-ray camera, suited to perform the 2D resolved X-Ray Fluorescence imaging of materials with high spatial and high-energy resolution, was designed and developed at the LANDIS laboratory. It consists of a CCD composed of 1024x1024 pixels (with a lateral size of 13.3 mm) coupled to a 70 mm laser-drilled pinhole collimator. The characteristic X-Ray fluorescence is induced on the samples under investigation, by irradiation with a medium-power X-ray tube.

In the present configuration, the pinhole camera works in a coaxial geometry. A maximum area of 5x4 cm^2 can be analyzed in a single measurement.

The analytical capabilities of the X-ray pinhole camera were accurately investigated. Energy response and energy calibration of the CCD detector was determined by irradiating pure target-materials. Measurements were performed by using a multi-frames acquisition in single-photon counting. The energy resolution measured at the Fe-K line was 157 eV. Spatial resolution of the pinhole camera was determined by analyzing the profile function of a sharp-edge at two testing values of magnification fixed at 3.2x and 0.8x. The spatial resolution was respectively of 90 mm and 190 mm.

A preliminary result of the application of the full field X-ray camera for performing the 2D resolved XRF imaging of material of interest in the cultural heritage field was presented.

References

[1] BUZANICH, G., RADTKE, M., REINHOLZ, U., RIESEMEIER, H., THÜNEMANN, A.F., STRELI, C., Impurities in multicrystalline silicon wafers for solar cells detected by synchrotron micro-beam X-ray fluorescence analysis, J. Anal. At. Spectrom. 27 (2012) 1875-1881.

[2] ROMANO, F.P., GARRAFFO, S., PAPPALARDO, L., RIZZO, F., In situ investigation of the surface silvering of late Roman coins by combined use of high energy broad-beam and low energy micro-beam X-ray fluorescence techniques, Spectrochim. Acta, Part B 73 (2012) 13–19.

[3] KANNGIEßER, B., MALZER, W., PAGELS, M., LÜHL, L., WESELOH, G., Three-dimensional micro-XRF under cryogenic conditions: a pilot experiment for spatially resolved trace analysis in biological specimens, Anal. Bioanal. Chem. 389 (2007) 1171-1176.

[4] SILVA, A.L.M., AZEVEDO, C.D.R., OLIVEIRA, C.A.B., DOS SANTOS, J.M.F., CARVALHO, M.L., VELOSO, J.F.C.A., Characterization of an energy dispersive X-ray fluorescence imaging system based on a Micropattern Gaseous Detector, Spectrochim. Acta Part B 66 (2011) 308–313.

[5] ALFELD, M., JANSSENS, K., SASOV, A., LIU, X., KOSTENKO, A., RICKERS-APPEL, K., FALKENBERG, G., The use of Full-Field XRF for simultaneous elemental mapping, AIP Conf. Proc. 1221 (2010) 111-118.

[6] SCHARF, O., IHLE, S., ORDAVO, I., ARKADIEV, V., BJEOUMIKHOV, A., BJEOUMIKHOVA, S., BUZANICH, G., GUBZHOKOV, R., GUNTHER, A., HARTMANN, R., KUHBACHER, M., LANG, X.M., LANGHOFF, N., LIEBEL, A., RADTKE, M., REINHOLZ, U., RIESEMEIER, H., SOLTAU, H., STRUDER, L., THUNEMANN, A.F., WEDELL, R., Compact pnCCD-Based X-ray Camera with High Spatial and Energy Resolution: A Color X-ray Camera, Anal. Chem. 83 (2011) 2532–2538.

[7] ROMANO, F.P., ALTANA, C., COSENTINO, L., CELONA, L., GAMMINO, S., MASCALI, D., PAPPALARDO, L., RIZZO, F., A new X-ray pinhole camera for energy dispersive X-ray fluorescence imaging with high-energy and high-spatial resolution, Spectrochim. Acta Part B, 2013, DOI 10.1016/j.sab.2013.04.012

Impressum

XRF Newsletter, No. 25, September 2013

The XRF Newsletter is prepared twice per year by the Nuclear Science and Instrumentation Laboratory of the IAEA Physics Section.
Correspondence and materials to be considered for publishing should be sent to:

Dr. Andreas G. Karydas
Nuclear Science and Instrumentation Laboratory, Physics Section
Division of Physical and Chemical Sciences
1400 Vienna, Austria
Fax: (+43-1) 2600 or (+43-1) 26007
E-Mail: A.Karydas@iaea.org

International Atomic Energy Agency
Vienna International Centre, PO Box 100, 1400 Vienna, Austria

Printed by the IAEA in Austria, February 2014

14-06711